



Glacial–interglacial changes of H<sub>2</sub><sup>18</sup>O, HDO and deuterium excess

M. Werner et al.

# Glacial–interglacial changes of H<sub>2</sub><sup>18</sup>O, HDO and deuterium excess – results from the fully coupled Earth System Model ECHAM5/MPI-OM

M. Werner<sup>1</sup>, B. Haese<sup>1,2</sup>, X. Xu<sup>1,3</sup>, X. Zhang<sup>1</sup>, M. Butzin<sup>1</sup>, and G. Lohmann<sup>1</sup>

<sup>1</sup>Alfred Wegener Institute, Helmholtz Centre for Polar and Marine Research, Bremerhaven, Germany

<sup>2</sup>Chair for Regional Climate and Hydrology, University of Augsburg, Germany

<sup>3</sup>Institute of Geosciences, Department of Geology, Kiel University, Germany

Received: 8 August 2015 – Accepted: 22 September 2015 – Published: 16 October 2015

Correspondence to: M. Werner (martin.werner@awi.de)

Published by Copernicus Publications on behalf of the European Geosciences Union.

Title Page

Abstract

Introduction

Conclusions

References

Tables

Figures



Back

Close

Full Screen / Esc

Printer-friendly Version

Interactive Discussion



## Abstract

In this study we present first results of a new isotope-enabled general circulation model setup. The model consists of a fully coupled atmosphere–ocean model ECHAM5/MPI-OM, enhanced by the interactive land surface scheme JSBACH and an explicit hydrological discharge scheme to close the global water budget. Stable water isotopes  $\text{H}_2^{18}\text{O}$  and HDO have been incorporated into all relevant model components. Results of two equilibrium simulations under pre-industrial and last glacial maximum conditions are analysed and compared to observational data and paleoclimate records for evaluating the model's performance of simulating spatial and temporal variations in the isotopic composition of the Earth's water cycle. For the pre-industrial climate, many aspects of the simulation results of meteoric waters are in good to very good agreement with both observations and earlier atmosphere-only simulations. The model is capable of adequately simulating the large spread in the isotopic composition of precipitation between low and high latitudes. A comparison to available ocean data also shows a good model-data agreement, however a strong bias of too depleted ocean surface waters is detected for the Arctic region. Simulation results under last glacial maximum boundary conditions also fit to the wealth of available isotope records from polar ice cores, speleothems, as well as marine calcite data. Data-model evaluation of the isotopic composition in precipitation reveals a good match of the model results and indicates that the temporal glacial–interglacial isotope–temperature relation was substantially lower than the present spatial gradient for most mid- to high-latitudinal regions. As compared to older atmosphere-only simulations, a remarkable improvement is achieved for the modelling of the deuterium excess signal in Antarctic ice cores. Our simulation results indicate that cool sub-tropical and mid-latitudinal sea surface temperatures are key for this progress. A recently discussed revised interpretation of the deuterium excess record of Antarctic ice cores in terms of marine relative humidity changes on glacial–interglacial timescales is not supported by our model results.

## Glacial–interglacial changes of $\text{H}_2^{18}\text{O}$ , HDO and deuterium excess

M. Werner et al.

Title Page

Abstract

Introduction

Conclusions

References

Tables

Figures



Back

Close

Full Screen / Esc

Printer-friendly Version

Interactive Discussion



## 1 Introduction

The water cycle is a key component of the Earth's climate system. Documenting and understanding its past evolution is essential to test our ability to model its future changes. Water stable isotopes ( $\text{H}_2^{18}\text{O}$ ,  $\text{HD}^{16}\text{O}$ , and  $\text{H}_2^{17}\text{O}$ ) are integrated tracers of climate processes occurring in various branches of this cycle (Craig and Gordon, 1965; Dansgaard, 1964). They have been successfully used to describe past climate changes for more than 30 years. For example, water stable isotopes (hereafter expressed in a  $\delta$ -notation as  $\delta^{18}\text{O}$  and  $\delta\text{D}$ , with respect to the Vienna Standard Mean Ocean Water standard V-SMOW, if not stated otherwise) have been measured routinely over the past decades in polar ice cores (Jouzel, 2013) and more recently also in non-polar ice cores (Hoffmann et al., 2003; Thompson et al., 1998). To a first order,  $\delta^{18}\text{O}$  and  $\delta\text{D}$  in polar ice cores are used for past temperature reconstructions over the past glacial–interglacial cycles (Jouzel et al., 2007; NEEM community members, 2013). In addition to high-resolution temperature records, the combination of water isotopic ratios permits to have a tracer of the low latitudes in polar ice cores. For other (sub-)tropical isotope archives, e.g. speleothems, some studies are indicating that the amount of precipitation could be mainly responsible for determining the water isotope concentration (Fleitmann et al., 2003; Wang et al., 2001) – this is called the amount effect (Dansgaard, 1964; Rozanski et al., 1992). Furthermore, in these regions  $\delta^{18}\text{O}$  and  $\delta\text{D}$  might also reflect convective activity along moisture trajectory (Vimeux et al., 2005; Yao et al., 2013). High resolution and well-dated records of  $\delta^{18}\text{O}$  of calcite in tropical speleothems in Asia or South America have therefore been interpreted in terms of past monsoon dynamics (Cruz et al., 2005; Wang et al., 2008). Analogously to continental speleothem archives, the seawater oxygen isotope concentration ( $\delta^{18}\text{O}_{\text{oce}}$ ) is conserved in carbonates ( $\delta^{18}\text{O}_{\text{oce}}$ ) from corals, foraminifers, and other marine species. Here, temperature during calcite formation and the isotopic composition of the seawater  $\delta^{18}\text{O}_{\text{oce}}$  are both the key factors controlling  $\delta^{18}\text{O}_{\text{c}}$  (Shackleton, 1974). Thus, carbonate isotope records from ocean sediment cores are fundamental records to access

**GMDD**

8, 8835–8894, 2015

### Glacial–interglacial changes of $\text{H}_2^{18}\text{O}$ , HDO and deuterium excess

M. Werner et al.

Title Page

Abstract

Introduction

Conclusions

References

Tables

Figures

◀

▶

◀

▶

Back

Close

Full Screen / Esc

Printer-friendly Version

Interactive Discussion





ship observed between modern annual mean precipitation isotope values and local annual mean temperature, precipitation amounts, or salinity, and for the atmosphere it is quantitatively consistent with a Rayleigh distillation process. However, this hypothesis is increasingly challenged (i) by new present-day observations, (ii) by alternative paleothermometry methods showing changing relationships for past periods (Buizert et al., 2014; Jouzel, 1999). This calls for a revised understanding of the interpretation of water stable isotopes, including second-order parameters such as deuterium excess, and their relationships with climatic conditions influencing the isotope signal.

One key tool for such an improved understanding of water isotopes in the Earth's hydrological cycle are atmospheric and oceanic general circulation models (GCM) with an explicit diagnostics of stable water isotopes. During the last three decades, several such isotope-enabled GCM have been built. Such models provide a mechanistic understanding of the physical processes influencing the isotopic composition of different water bodies in the climate system. They allow the explicit simulation of isotopic fractionation processes during any phase changes of a water mass within the model's hydrological cycle, e.g. during evaporation of water from land or ocean surface, cloud droplet formation, and re-evaporation of droplet water below cloud base. In such an isotope-enabled GCM setup, all relevant factors determining the strength and variability of isotopic fractionation are known.

The early implementations of water stable isotopes in atmospheric models (Hoffmann et al., 1998; Joussaume et al., 1984; Jouzel et al., 1987) have already shown their potential in explaining fundamental physical hydroclimate relationships. Since then, considerable progress has been made in simulating stable water isotopes in climate models, as the climate models have evolved themselves (Risi et al., 2010b; Werner et al., 2011). Using atmospheric models, water stable isotopes have been used for a considerable range of applications at small spatial and temporal scales such as investigating the link between water stable isotopes and decadal variability (Kurita et al., 2011) or to analyse mixing processes within rain events (Lee et al., 2009; Risi et al., 2010a). Many of these atmospheric GCM include at least two stable water iso-

## GMDD

8, 8835–8894, 2015

### Glacial–interglacial changes of $H_2^{18}O$ , HDO and deuterium excess

M. Werner et al.

Title Page

Abstract

Introduction

Conclusions

References

Tables

Figures

◀

▶

◀

▶

Back

Close

Full Screen / Esc

Printer-friendly Version

Interactive Discussion



**Glacial–interglacial changes of H<sub>2</sub><sup>18</sup>O, HDO and deuterium excess**

M. Werner et al.

[Title Page](#)[Abstract](#)[Introduction](#)[Conclusions](#)[References](#)[Tables](#)[Figures](#)[Back](#)[Close](#)[Full Screen / Esc](#)[Printer-friendly Version](#)[Interactive Discussion](#)

topes (oxygen-18 and deuterium). With the improvements of the atmospheric GCM in simulating present-day water isotopic content, part of the interest has lately shifted to second order content such as deuterium excess and <sup>17</sup>O excess that can provide further constraints on the water cycle but remains challenging (Risi et al., 2010b; Werner et al., 2011). Besides building atmospheric isotope-enabled GCM, several international groups have also worked on the inclusion of the water isotopes in oceanic GCM. Here, the water isotopic content is a passive tracer once the surface oceanic conditions are determined through the water balance with the atmosphere and the additional fractionation during sea-ice formation and melting. Attempts in oceanic-only GCM have proven useful to challenge the link between oceanic water isotopic content and salinity (Delaygue et al., 2000; Paul et al., 1999; Schmidt, 1998), a subject of considerable interest in paleoceanography.

In general, simulating evolving climate conditions requires using self-contained climate models as much as possible, to avoid prescribing unnecessary or unknown boundary conditions. In particular for past climates applications, it is necessary to simulate stable water isotopes in the full water cycle system, not only in its atmospheric part. So far however, few studies have used fully coupled isotope-enabled climate general circulation models to address questions related to the water cycle. Schmidt et al. (2007) incorporated water isotopes within the water cycle of the Goddard Institute for Space Studies (GISS) coupled ocean-atmosphere model (ModelE). In several multi-centennial simulations, they examined the internal variability and the simulated changes due to orbital and greenhouse gas forcing. Their study was restricted to the modern (preindustrial) and mid-Holocene (6 kyr B.P.) climates. LeGrande et al. (2009) expanded these analyses by performing eight Holocene time slice simulations, each ~ 1000 years apart. Lewis et al. (2010) used the same GISS-E model for simulating the consequences of a large freshwater input into the North Atlantic as an idealized analogue to iceberg discharge during Heinrich events. As a second fully coupled GCM, the HadCM3 model, has been enhanced by a stable water isotope diagnostics module by Tindall et al. (2009) for analyses of the present-day isotopic signature of El Niño –

## Glacial–interglacial changes of H<sub>2</sub><sup>18</sup>O, HDO and deuterium excess

M. Werner et al.

Title Page

Abstract

Introduction

Conclusions

References

Tables

Figures



Back

Close

Full Screen / Esc

Printer-friendly Version

Interactive Discussion



Southern Oscillation and the tropical amount effect. Besides these two fully coupled isotope-enabled GCM, there have also been some efforts in including water stable isotopes in the hydrological cycle of Earth System Models of Intermediate Complexity (EMICs) by Roche et al. (2004), Brennan et al. (2012), as well as Roche and Caley (2013). These isotope-enabled EMICs can be classified as an alternative tool to test ideas, explore large periods of time in a transient mode and guide much more computationally demanding simulations with fully coupled GCM.

The Paleoclimate Modeling Intercomparison Project (PMIP, <http://pmip3.lsce.ipsl.fr>) has chosen the Last Glacial Maximum (LGM) climate as one of the target periods for the evaluation of GCM modelling results. The LGM climate is not only very different from the present and/or pre-industrial climate, but this latest glacial epoch offers also a wealth of terrestrial, marine, and ice core proxy data for an in-depth model-data comparison. As many of these data sets are based on water stable isotopes (e.g., speleothem data, marine calcite data, ice core records) several studies with isotope-enabled GCM have also chosen the LGM as a key period for an evaluation of modelled  $\delta^{18}\text{O}$  and  $\delta\text{D}$  values with different proxy data (Jouzel et al., 2000; Lee et al., 2008; Lewis et al., 2013; Risi et al., 2010b).

Here we present first results of a newly developed isotope-enhanced version of the fully coupled GCM ECHAM5/MPI-OM. The model amalgamates our previous efforts to include stable water isotope diagnostics within the atmosphere GCM ECHAM5 (Werner et al., 2011), the land surface scheme JSBACH (Haese et al., 2013), as well as the ocean GCM MPI-OM (Xu et al., 2012). Our following analysis and presentation of simulation results focus on the following questions: (a) How well does this fully coupled Earth System Model simulate first-order isotopic variations ( $\delta^{18}\text{O}$ ,  $\delta\text{D}$ ) within different parts of the Earth's water cycle under pre-industrial and LGM, defined as the period 23 000–19 000 years before present, boundary conditions? (b) Do the model results indicate substantial changes of the temperature–isotope relation of meteoric water? (c) Are simulated spatial and temporal variations of the deuterium excess in precipitation, a second-order isotope effect, also in agreement with available observations and pa-

leoproxy data? (d) If so, how are these variations of deuterium excess related to past changes of evaporation processes?

## 2 Model components and simulation setup

### 2.1 Model components

5 In this study we use the Earth System Model ECHAM5/MPIOM, formerly also named as Community Earth System Model COSMOS. It is a fully coupled ocean-atmosphere-sea ice-land surface model (Jungclaus et al., 2006), which has now been enhanced by stable water diagnostics in all relevant model components. Previous studies with the standard (non-isotope) version of COSMOS have applied and evaluated this model, among others, for the pre-industrial climate (Wei et al., 2012), glacial and interglacial climate states (Zhang et al., 2014, 2013), the Holocene (Wei and Lohmann, 2012) and Cenozoic climate change (Knorr et al., 2011; Stepanek and Lohmann, 2012).

15 During the recent years, all key model components (ECHAM5, MPI-OM, JSBACH) have been equipped with a diagnostic module to explicitly simulate both  $\text{H}_2^{18}\text{O}$  and HDO within the different parts of the hydrological cycle. Here, we give just a brief summary of key model components and isotope implementation within them and refer to previous publications for details.

20 The atmosphere component of our model setup is the ECHAM5 atmosphere GCM, which has been mainly built at the Max Planck Institute for Meteorology, Hamburg. The model has a spectral, dynamical core, which is constrained by the equations of state describing the conservation of mass, energy, and momentum. Further model constraints are set by the continuity equation, a prediction equation for the surface pressure, as well as the hydrostatic equation (Roeckner et al., 2003). The water cycle in ECHAM5 contains formulations for evapotranspiration of terrestrial water, evaporation of ocean water, and the formation of large-scale and convective clouds. Within the atmosphere's advection scheme, vapour, liquid and frozen water are transported in-

## Glacial–interglacial changes of $\text{H}_2^{18}\text{O}$ , HDO and deuterium excess

M. Werner et al.

Title Page

Abstract

Introduction

Conclusions

References

Tables

Figures

◀

▶

◀

▶

Back

Close

Full Screen / Esc

Printer-friendly Version

Interactive Discussion





## Glacial–interglacial changes of H<sub>2</sub><sup>18</sup>O, HDO and deuterium excess

M. Werner et al.

Title Page

Abstract

Introduction

Conclusions

References

Tables

Figures

◀

▶

◀

▶

Back

Close

Full Screen / Esc

Printer-friendly Version

Interactive Discussion



dependently. A detailed model description is given in Roeckner et al. (2003, 2006). Stable water isotopes have been implemented into ECHAM5 in an analogous manner to previous ECHAM model releases (Hoffmann et al., 1998; Werner and Heimann, 2002). The isotope module in ECHAM5 computes the isotopic signal of different water masses within the entire water cycle. Details of the implementation have been reported in Werner et al. (2011). In the atmosphere–ocean coupled setup, ECHAM5 provides the required freshwater flux (P–E) and its isotopic composition for all ocean grid cells to the ocean model MPI-OM.

Within the ECHAM5 model setup used in this study, the JSBACH land surface model calculates the boundary conditions for ECHAM5 over terrestrial areas. This includes the exchange of water, energy, and momentum between the land surface and the atmosphere (Raddatz et al., 2007). JSBACH divides each land surface grid cell into 8 tiles covered by different plant functional types and bare soil. The simulated dynamical vegetation changes are controlled by the processes of natural growing and mortality, as well as disturbance mortality (e.g., wind, fire). Details of this approach are described in Brovkin et al. (2009). The water isotopes H<sub>2</sub><sup>18</sup>O and HDO are almost passive tracers in the JSBACH model. No fractionation of the isotopes is assumed during most physical processes partitioning water masses on the land surface (e.g., snow melt, formation of surface water runoff and drainage; see Haese et al., 2013 for details). For evapotranspiration, fractionation of isotopes might occur during evaporation of water from bare soils. However, the strength of this fractionation remains an open question. In accordance with the results of Haese et al. (2013), we assume in this study that we can ignore any possible fractionation during evapotranspiration processes from terrestrial areas, as our analyses will focus primarily on the isotopic composition of precipitation. This choice might add a small bias to the isotopic composition of terrestrial surface water pools and the discharge of terrestrial net precipitation (P–E) towards the oceans.

In the used coupled model setup, terrestrial water discharge to the ocean is calculated by the so-called Hydrological Discharge scheme (HD scheme; Hagemann and Gates, 2003). Modelled discharge is calculated with respect to the slope of the to-

## Glacial–interglacial changes of H<sub>2</sub><sup>18</sup>O, HDO and deuterium excess

M. Werner et al.

[Title Page](#)

[Abstract](#)

[Introduction](#)

[Conclusions](#)

[References](#)

[Tables](#)

[Figures](#)

[⏪](#)

[⏩](#)

[◀](#)

[▶](#)

[Back](#)

[Close](#)

[Full Screen / Esc](#)

[Printer-friendly Version](#)

[Interactive Discussion](#)



pography. For the simulated total river runoff it is assumed that the global water cycle is closed, i.e., all net precipitation (P–E) over terrestrial areas is transported to the ocean. However, lakes are absent in the HD scheme. This may lead to minor errors in the magnitude and location of the modelled river runoff compared to observations.  
5 As the ECHAM5/MPI-OM coupled model setup does not include a dynamic ice sheet model, precipitation amounts falling on glaciers are instantaneously put as runoff into the nearest ocean grid cell for closing the global water budget. Independent of the chosen spatial ECHAM5 model resolution, the HD scheme is always implemented on a fine horizontal 0.5° × 0.5° degree grid and allows simulating water mass flows of the major  
10 river systems of the Earth. Stable water isotopes H<sub>2</sub><sup>18</sup>O and HDO are incorporated as passive tracers within the HD scheme.

The ocean component of our model setup consists of the general circulation model MPIOM (Marsland et al., 2003), which is employed on a curvilinear Arakawa-C grid. The used MPIOM setup has a free surface and contains subgrid-scale parameterizations for convection, vertical and isopycnal diffusivity, horizontal and vertical viscosity,  
15 as well as for the bottom boundary layer flow across steep topography. Sea ice is simulated by a viscous-plastic rheology model (Hibler, 1979). It considers thermodynamic sea ice melt and growth, and also a thermohaline coupling by brine rejection. Within MPI-OM, H<sub>2</sub><sup>18</sup>O and HDO are treated as passive tracers. They are fully mixed and ad-  
20 vected within the model, and their total mass is conserved. Isotopic variations occur mainly due to temperature-dependent isotope fractionation during evaporation, as well as by advection and mixing of different water masses. Changes of the oceanic water masses by terrestrial freshwater fluxes entering the ocean are included in the model setup, too. For the process of sea ice formation from liquid waters, the isotopic composition of sea ice is calculated by a liquid to ice equilibrium fractionation factor of  
25 1.003, which is the average of various estimates (Craig and Gordon, 1965; Lehmann and Siegenthaler, 1991; Macdonald et al., 1995; Majoube, 1971). Due to the very low rate of isotopic diffusion in sea ice, we assume no fractionation during sea ice melting. In the atmosphere–ocean coupled setup, MPI-OM provides the isotope composition

of sea surface water and sea ice as a temporally varying boundary condition to the atmosphere model ECHAM5.

Within ECHAM5/MPI-OM, atmosphere and ocean are coupled via the Ocean–Atmosphere–Sea Ice–Soil OASIS3 coupler (Valcke et al., 2003). Mass, energy, and momentum fluxes, as well as the related isotope masses of  $\text{H}_2^{18}\text{O}$  and HDO, are exchanged between the atmosphere and ocean once per day. The coupling is described in detail in Jungclaus et al. (2006).

## 2.2 Simulation setup

We have used the following simulation setup for all simulation results presented in this study: the atmospheric component ECHAM5 runs at a horizontal resolution of approx.  $3.75^\circ \times 3.75^\circ$  with 19 vertical levels between surface and 10 hPa (T31L19 resolution). The same horizontal resolution is applied for the land surface scheme JSBACH. The ocean model MPI-OM has a formal horizontal resolution of approx.  $3^\circ \times 1.8^\circ$  and 40 uneven vertical layers on z-levels. The used MPI-OM model setup has a bipolar orthogonal spherical coordinate system, where the poles are placed over Greenland and Antarctica, respectively. Placing one pole over Greenland avoids a grid singularity in the Arctic Ocean. Furthermore, it ensures a high horizontal grid resolution in the deep-water formation regions of the northern North Atlantic Ocean and the Arctic.

Two different simulations were performed, one for the pre-industrial and one for the LGM climate. We briefly describe here these experimental setups: for the pre-industrial (PI) climate, ECHAM5/MPI-OM has been continued from a PI simulation without isotopes included, which has been in run into equilibrium over several thousand years (Wei et al., 2012; Zhang et al., 2013) using identical PI boundary conditions. At model start, isotope values in the atmosphere have been set to constant values ( $\delta^{18}\text{O}$ :  $-10\text{‰}$ ,  $\delta\text{D}$ :  $-80\text{‰}$ ), while the oceanic isotope distribution has been taken from an equilibrium run over 3000 years with the MPI-OM-wiso ocean model (Xu, 2012) with global mean  $\delta^{18}\text{O}$  and  $\delta\text{D}$  values of  $0\text{‰}$ , each (Baertschi, 1976; de Wit et al., 1980). The fully coupled ECHAM5/MPI-OM model with included isotope diagnostics has then been

GMDD

8, 8835–8894, 2015

## Glacial–interglacial changes of $\text{H}_2^{18}\text{O}$ , HDO and deuterium excess

M. Werner et al.

Title Page

Abstract

Introduction

Conclusions

References

Tables

Figures

◀

▶

◀

▶

Back

Close

Full Screen / Esc

Printer-friendly Version

Interactive Discussion



## Glacial–interglacial changes of H<sub>2</sub><sup>18</sup>O, HDO and deuterium excess

M. Werner et al.

Title Page

Abstract

Introduction

Conclusions

References

Tables

Figures

◀

▶

◀

▶

Back

Close

Full Screen / Esc

Printer-friendly Version

Interactive Discussion



run under PI boundary conditions (orbital forcing, greenhouse gas concentrations, ocean bathymetry, land surface and ice sheet topography) for another 1400 years. For the LGM simulation, we impose orbital forcing and greenhouse gas concentrations (CO<sub>2</sub>=185 ppm; N<sub>2</sub>O = 200 ppb; CH<sub>4</sub>=350 ppb) as well as surface boundary conditions (terrestrial topography, ocean bathymetry, runoff routes according to ice sheet reconstruction) in accordance with the PMIP3 protocol (<http://pmip3.lsce.ipsl.fr/>). An increased global salinity (1 PSU added compared to modern values) accounts for a LGM sea level drop of approx. 116 m. Again, the isotope-enabled version of ECHAM5/MPI-OM has been restarted from an already equilibrated simulation without isotopes (Zhang et al., 2013). The initial LGM oceanic H<sub>2</sub><sup>18</sup>O and HDO distribution has been taken from a 3000 year long MPI-OM-wiso integration under LGM boundary conditions (Xu, 2012) with a prescribed glacial increase of δ<sup>18</sup>O of +1 ‰ (δD: +8 ‰). The fully coupled ECHAM5/MPI-OM model with included isotope diagnostics has then been run for another 1300 years.

At the end of the PI and LGM simulation period, none of the two runs shows any trend in the isotopic composition of ocean surface waters, and δ<sup>18</sup>O (δD) trends in deep ocean waters at 2200 m are smaller than 0.005 ‰ 100 yr<sup>-1</sup> (0.05 ‰ 100 yr<sup>-1</sup>). Thus, we rate both simulations as equilibrated and consider the last 100 model years for our analyses.

If not stated otherwise, all reported δ values of meteoric waters (precipitation, evaporation) in this study are calculated as precipitation (or evaporation)-weighted averages with respect to the V-SMOW scale. The δ values of ocean waters are calculated as arithmetic averages with respect to the V-SMOW scale.

### 3 Observational data

#### 3.1 GNIP and GISS database

The Global Network of Isotopes in Precipitation (GNIP) was initiated in 1958 by IAEA and WMO, and became operational in 1961 (IAEA/WMO, 2010). Since then, monthly samples of  $\text{H}_2^{18}\text{O}$  and HDO in precipitation have been sampled at more than 900 stations from more than 100 different countries. While several stations have continuously collected samples for two or more decades (e.g., GNIP stations in Krakow, Ottawa, Reykjavik, and Vienna), many other GNIP stations have been in operation for a much shorter period, only. Here, we use a subset of 70 stations from the GNIP database, where surface temperature, precipitation,  $\delta^{18}\text{O}$ , and  $\delta\text{D}$  have been reported for a minimum of 5 calendar years, any time within the period 1961 to 2007.

The GISS global seawater oxygen-18 database (Schmidt et al., 1999) is a collection of over 26 000 seawater  $\text{O}^{18}$  values made since about 1950. Partial versions of this database already appeared in Schmidt (1999) and Bigg and Rohling (2000). From this database we are using only values with no applied correction (see Schmidt et al., 1999 for details of the applied corrections). It is important to note that, in contrast to GNIP  $\delta^{18}\text{O}$  values of precipitation, GISS  $\delta^{18}\text{O}$  values in ocean water do not represent annual mean values, but are typically measured from a sample taken during an arbitrary day of the year. Therefore, we compare in this study the GISS data not to simulated annual mean isotope values in ocean waters, but to the long-term mean monthly value of the specific month, when a GISS  $\delta^{18}\text{O}$  value was reported.

#### 3.2 Ice core data

In the late 1960s Dansgaard (1969), Lorius (1979) and others started their pioneering work of analysing polar ice cores for climate research. Since then, the isotopic composition of more than a dozen deep ice cores both from Greenland and Antarctica has been measured. In parallel, alpine ice cores from (sub)tropical regions of South Amer-

## GMDD

8, 8835–8894, 2015

### Glacial–interglacial changes of $\text{H}_2^{18}\text{O}$ , HDO and deuterium excess

M. Werner et al.

Title Page

Abstract

Introduction

Conclusions

References

Tables

Figures

⏪

⏩

◀

▶

Back

Close

Full Screen / Esc

Printer-friendly Version

Interactive Discussion



## Glacial–interglacial changes of $H_2^{18}O$ , HDO and deuterium excess

M. Werner et al.

Title Page

Abstract

Introduction

Conclusions

References

Tables

Figures

⏪

⏩

◀

▶

Back

Close

Full Screen / Esc

Printer-friendly Version

Interactive Discussion



ica (Hoffmann et al., 2003; Thompson et al., 1995), Africa (Thompson et al., 2002), and the Tibetan Plateau (Thompson et al., 1989; Tian et al., 2003; Yao et al., 2012) have been drilled and analysed during the last decades, too. In this study we use a subset of 6 Greenland, 10 Antarctic, and 5 (sub)tropical ice cores to compare the measured  $\delta^{18}O$  and  $\delta D$  values for the pre-industrial climate and the LGM with our simulation results. For the different ice core records, we take the minimum  $\delta^{18}O$  ( $\delta D$ , dex) value of the time interval 19 000 to 23 000 B.P. as a representative mean LGM  $\delta^{18}O$  ( $\delta D$ , dex) value. The ice core data used in this study is summarized in Table 1.

### 3.3 Speleothem calcite data

Recently, Shah et al. (2013) have published a global synthesis of speleothem  $\delta^{18}O$  records spanning the period from the LGM until present, which consists of data from 60 speleothems of 36 different sites. From this compilation we have selected a subset of 8 speleothem records (Table 2), where 1000 years-averaged  $\delta^{18}O$  values calculated by Shah et al. are available for both the LGM (defined here as period 19 000 to 22 000 years B.P.) and the most recent 1000 years B.P. We use the latter as representative mean PI  $\delta^{18}O$  values at the different locations. We are aware that during the last 1000 years B.P. the climate at a specific speleothem site might have been variable and different from the pre-industrial climate of our ECHAM5/MPI-OM simulation, which could lead to a bias in the model-data comparison. We are also aware that drip water in a cave, which isotopic composition is archived in a speleothem record, might be seasonally biased due to re-evaporation of the precipitated water (Wackerbarth et al., 2010). Furthermore, for many speleothems an additional fractionation between the drip water and the formed calcite can be observed (Dreybrodt and Scholz, 2011). Thus, necessary caution will be taken for the comparison of model results with the selected speleothem data.

All listed  $\delta^{18}O$  data in Table 2 are measured isotope values in carbonate and refer to the Pee Dee Belemnite (PDB) standard. For comparison with model results, we use a formula linking  $\delta^{18}O$  in water and  $\delta^{18}O$  in speleothem calcite, derived by Kim and

O'Neil (1997) for synthetic calcite:

$$\delta^{18}\text{O}_{\text{c(SMOW)}} = \delta^{18}\text{O}_{\text{water(SMOW)}} + 18.03 \times (1000/T) - 32.17$$

with  $T$  being the temperature (in Kelvin) during calcite formation. Conversion between  $\delta^{18}\text{O}$  values on PDB and SMOW scale is calculated as suggested by Coplen (1988):

$$\delta^{18}\text{O}_{\text{PDB}} = 0.97002 \times \delta^{18}\text{O}_{\text{SMOW}} - 29.98$$

### 3.4 Marine calcite data

Caley et al. (2014) have recently compiled and published a marine calcite  $\delta^{18}\text{O}$  data set from 114 (115) pairs of deep-sea cores, which contain both LGM and late Holocene planktic (benthic) foraminifera  $\delta^{18}\text{O}$  data. In their study they report  $\delta^{18}\text{O}$  anomalies as the change between mean  $\delta^{18}\text{O}$  values of the period 19 000 to 23 000 years B.P. and over the last 3000 years of each record. The MARGO project definition has been used to assure chronostratigraphic quality of the selected data (Kucera et al., 2005). Planktic foraminifera data have been mainly measured in the following species: *Globigerinoides sacculifer*, *Globigerinoides ruber* pink and white, *Neogloboquadrina pachyderma sinistral*, and *Globigerina bulloides*. Benthic foraminifera data includes, among others, *Cibicidoides wuellerstorfi*, *Cibicidoides pachyderma*, and *Cibicidoides peregrina*. For a more detailed description of this data set we refer to Caley et al. (2014).

According to Shackleton (1974) the  $\delta^{18}\text{O}_{\text{c}}$  signal in calcite shells of planktic and benthic foraminifera can be interpreted by the following expression relating temperature to the equilibrium fractionation of inorganic calcite precipitation around 16.9 °C:

$$T = 16.9 - 4.38 \times \left( \delta^{18}\text{O}_{\text{c(PDB)}} - \delta^{18}\text{O}_{\text{oce(SMOW)}} \right) + 0.1 \times \left( \delta^{18}\text{O}_{\text{c(PDB)}} - \delta^{18}\text{O}_{\text{oce(SMOW)}} \right)^2$$

with  $T$  being the temperature during calcite formation,  $\delta^{18}\text{O}_{\text{c(PDB)}}$  the isotopic composition of calcite on the PDB scale, and  $\delta^{18}\text{O}_{\text{oce(SMOW)}}$  the isotopic composition of seawater on the SMOW scale.

Title Page

Abstract

Introduction

Conclusions

References

Tables

Figures

⏪

⏩

◀

▶

Back

Close

Full Screen / Esc

Printer-friendly Version

Interactive Discussion







sphere model, and the deviations can partly be explained by the coarse T31L19 model resolution (Werner et al., 2011). Similar distributions of  $\delta^{18}\text{O}$  and  $\delta\text{D}$  in precipitation have been reported for several atmosphere-only and fully coupled GCM during the last years (e.g., Lee et al., 2007; Risi et al., 2010b; Schmidt et al., 2007; Tindall et al., 2009).

5 While all these models show a reasonable resemblance to GNIP observations for the large-scale patterns in low- and mid-latitudinal regions, some models have difficulties to correctly simulate the very low temperatures and strong isotope depletions over the Antarctic ice sheet (e.g., Lee et al., 2007).

#### 4.1.2 Isotopes in ocean waters

10 In Fig. 2a, the simulated annual mean  $\delta^{18}\text{O}_{\text{oce}}$  signal in ocean surface waters (mean over the depth interval between surface and 10 m) are plotted. Mean values in the tropical to mid-latitudinal oceans range between +0.05‰ to +1.2‰, with a tendency to higher values in the Atlantic Ocean as compared to the Pacific and Indian Ocean. This relative enrichment can be explained by a net freshwater export of Atlantic Ocean water, which is transported westwards to the Pacific (Broecker et al., 1990; Lohmann, 2003; Zaucker and Broecker, 1992). The highest enrichment in the Atlantic Ocean is found south of Bermuda Island with surface water  $\delta^{18}\text{O}_{\text{oce}}$  values of up to +1.3‰.

15 Other, more localized regions of surface water  $\delta^{18}\text{O}_{\text{oce}}$  enrichment with a similar order of magnitude are the Mediterranean Sea, the Black Sea, as well as the Red Sea. Again, this enrichment is most likely caused by a regional surplus of evaporation vs. precipitation in these three regions. Stronger than average depletion of  $\delta^{18}\text{O}_{\text{oce}}$  surface waters is simulated for both high-latitudinal ocean regions. While surface waters in the Southern Ocean between 50–75° S show a depletion of down to –0.8‰, modelled surface waters in the Arctic Ocean are depleted by down to –1.6‰. This depletion is most likely caused by two effects: (a) the implemented fractionation during sea ice formation which leads to an enrichment (depletion) of the isotopes in sea ice (the remaining liquid water); (b) the inflow of highly depleted water masses of Arctic rivers in combination with a strong stratification of the simulated Arctic Ocean water masses (see below).

25

## Glacial–interglacial changes of $\text{H}_2^{18}\text{O}$ , HDO and deuterium excess

M. Werner et al.

Title Page

Abstract

Introduction

Conclusions

References

Tables

Figures

◀

▶

◀

▶

Back

Close

Full Screen / Esc

Printer-friendly Version

Interactive Discussion



For a quantitative evaluation of the model results, we compare the simulated values to 3859  $\delta^{18}\text{O}$  entries of the selected GISS data (Chapter 3.1), which represent surface ocean water values between surface and 10 m depth. On a global scale, the simulated  $\delta^{18}\text{O}_{\text{oce}}$  values agree quite well within a range of  $\pm 0.25\text{‰}$  with the GISS values (Fig. 2b). Strongest model-data deviations are found in the following regions: (a) In the vicinity of several large river estuaries the model results reveal too high  $\delta^{18}\text{O}_{\text{oce}}$  values (e.g., at the Amazon and Ganges river mouths); (b) the model also overestimates  $\delta^{18}\text{O}_{\text{oce}}$  in surface water in the Baltic Sea as well as in the Black Sea; (c) for the Arctic Ocean region the comparison yields mixed results: while the MPI-OM model tends to overestimate  $\delta^{18}\text{O}_{\text{oce}}$  in ocean surface waters in some regions by more than  $+2\text{‰}$  (e.g. the eastern coast of Greenland, and in the Beaufort Sea north of Alaska), in most other Arctic regions the model results are lower by more than  $-2\text{‰}$  than the GISS observations (e.g., in the Hudson Bay area, and the Barents Sea, the Kara Sea, as well as the Laptev Sea).

A separation of the model-data comparison into Atlantic, Pacific, Indian, and Arctic Ocean, does not show any systematic deviations between modelled  $\delta^{18}\text{O}_{\text{oce}}$  values and the GISS data for the first three oceans (Fig. 3). We find strong correlations between modelled values and the GISS data as well as a RMSE below 1% for all 3 oceans (Atlantic:  $n = 458$ ,  $r^2 = 0.90$ , RMSE = 0.77; Pacific:  $n = 736$ ,  $r^2 = 0.62$ , RMSE = 0.72, Indian Ocean:  $n = 345$ ,  $r^2 = 0.46$ , RMSE = 0.46). The strongest deviations of model values from observational data are caused by the overestimation of  $\delta^{18}\text{O}_{\text{oce}}$  values near river estuaries, at the Baltic Sea, and at the Sea of Okhotsk. For the Arctic Ocean, the majority of the simulated  $\delta^{18}\text{O}_{\text{oce}}$  values is stronger depleted than the corresponding GISS entries and the model-data correlation is worse ( $n = 410$ ,  $r^2 = 0.35$ , RMSE = 2.12). This bias in our ECHAM5/MPI-OM model is most likely caused by a too stratified Arctic Ocean. Highly depleted water inflowing from Arctic rivers remains in the upper layers of the Arctic Ocean and is not well mixed with deeper waters. This model deficit is clearly depicted in a comparison of the mean modelled isotope signal with available measurements from the GISS database in meridional

sections of the Atlantic (zonal mean between 60–0° W; Fig. 4a) and the Pacific basin (zonal mean of region 150° E to 110° W; Fig. 4b). For both cross sections, we find that the overestimated depletion of  $\delta^{18}\text{O}_{\text{oce}}$  values in the Arctic reaches down to approx. 500 m below the surface while simulated North Atlantic Deep Water (NADW) masses are less depleted and in better agreement with the GISS data. Similar low isotope values in the Arctic oceans have already been reported by former studies with ocean-only GCM (Paul et al., 1999; Xu et al., 2012).

In general, we find for the Atlantic Ocean a fair agreement between GISS observations and model values. The regions of the strongest enrichment is located between 40° S to 30° N, with maximum enrichment (+0.6‰ or more) at approx. 20° S to 30° N, and a decreasing trend of enrichment in deeper water until approx. +0.1‰ at a depth of 3000 m. The enriched water masses are also found in NADW below 1000 m, with an enrichment of up to +0.2‰ (Fig. 4a). On the contrary, Atlantic water masses south of 40° S show a relative depletion down to –0.4‰ in their isotopic signature for all water depth, in agreement with available GISS data. Depleted water masses stemming from the Antarctic Bottom Water (AABW) are reaching until the equator where the isotopic signal is then mixed with NADW and enriched tropical Atlantic waters. For the Pacific (Fig. 4b) we find a similar vertical and latitudinal  $\delta^{18}\text{O}_{\text{oce}}$  distribution as in the upper layers of the Atlantic Ocean, while the transition zone between enrichment and depletion shoals to approx. 1000 m water depth. Below a depth of approx. 3500 m, depleted AABW ( $\delta^{18}\text{O}_{\text{oce}}$  between –0.4 and –0.1‰) fills the entire Pacific. The overall pattern of the Atlantic and Pacific cross sections is in good agreement with a recent study of the *i*LOVECLIM isotope-enabled EMIC (Roche and Caley, 2013) as well as with two ocean-only GCM studies (Paul et al., 1999; Xu et al., 2012).

### 4.1.3 Discharge of terrestrial surface water

In Fig. 5a, we show the simulated annual mean values of  $\delta^{18}\text{O}$  for grid cells with a mean inflow of at least  $200\text{ m}^3\text{ s}^{-1}$ , as simulated by the HD scheme (see Chapter 2.1), to depict the major river systems on Earth, only. In general, the isotopic composition of

Title Page

Abstract

Introduction

Conclusions

References

Tables

Figures

⏪

⏩

◀

▶

Back

Close

Full Screen / Esc

Printer-friendly Version

Interactive Discussion



## Glacial–interglacial changes of $H_2^{18}O$ , HDO and deuterium excess

M. Werner et al.

Title Page

Abstract

Introduction

Conclusions

References

Tables

Figures

◀

▶

◀

▶

Back

Close

Full Screen / Esc

Printer-friendly Version

Interactive Discussion



a specific river is closely linked to the  $\delta^{18}O$  signal of P–E in the catchment area of the particular river. The strongest depletion of  $-12\%$  or less is found for river systems of in high northern regions of Siberia and Alaska, in agreement with observational data (Dodd et al., 2012). For the Rhine, the simulated isotopic composition in the Netherlands is about  $-7$  to  $-8\%$ , in good agreement with available observations, and similar good agreement is found for the Mackenzie River in the Canadian Arctic with a modelled outflow signal of  $-19$  to  $-20\%$  (Hoffmann et al., 1998). Rivers in mid- and low latitudes contain in general more enriched waters, and the PI model experiment results in least depleted waters ( $> -4\%$ ) for the Paraná River (Argentina), and the Orange River (South Africa). In the future, the current efforts of the IAEA to build a systematic database of available isotope measurements in rivers (IAEA, 2012) will allow for a more thoroughly evaluation of these model results.

For closing the global water budget, the HD scheme does not only simulate the water transport via large river systems, but also redistributes all net surplus water of terrestrial P–E fluxes to a nearby coastal grid point by following orographic gradients. The  $\delta^{18}O$  values of the resulting annual mean water inflow of the coastal grid points to the ocean is shown in Fig. 5b.

### 4.1.4 Deuterium excess in meteoric and ocean surface waters

In Fig. 6 we show the simulated dex signal in evaporation, precipitation, and ocean surface waters. Dex values in evaporation (Fig. 6a) range between  $-2$  and  $+16\%$ . The lowest values are found in extreme cold and windy regions of the Arctic, parts of the North Atlantic and above surface waters of the Antarctic Circumpolar Current (ACC). Further negative dex values are simulated for parts of the Sahara and the Arabian Peninsula, but these values occur in regions of extreme low evaporation fluxes from the terrestrial surface and are not meaningful but represent numerical artefacts, caused by the division of two small numerical values for calculating the  $\delta^{18}O$  and  $\delta D$  values. Maximum dex values of up to  $+14\%$  are detected in various regions of the Earth, both

above terrestrial and marine surfaces. It is very difficult to evaluate this simulated pattern of dex in evaporation, as no systematic data collection of this quantity exists, so far. For precipitation (Fig. 6b), modelled dex<sub>p</sub> values range between 0 and +18‰ with the highest values in northern parts of the Sahara and a band-like structure covering the mountain regions of Iraq, the Hindu Kush and large parts of the Himalayan plateau. The lowest values occur in dry regions of the southern Sahara and the Arabian Peninsula, northern India, and northern Brazil. The Southern Ocean is another region with simulated low dex<sub>p</sub> values. For the Antarctic continent, the large-scale dipole of low (high) dex values in West (East) Antarctica is well captured by the model. For ocean surface waters (Fig. 6d), the simulated variations in deuterium excess are an order of magnitude lower than in precipitation and range between -1.6 and +1.6‰. Model results reveal a clear distinction with rather low dex values in mid- to low-latitude Atlantic regions, the highest dex values in the Arctic Ocean and the Baltic Sea, and rather small variations ( $\pm 0.4\%$ ) in the remaining oceans. Both positive and negative anomalies are directly linked to the hydrological balance in the particular regions: in the low- to mid-latitude Atlantic Ocean, a net freshwater export exists. As the evaporated and exported water masses have a positive dex composition, the remaining ocean surface waters will become negative in their dex composition due to mass balance. In opposite, a region like the Baltic Sea has a positive mass balance, i.e. total P-E from the Baltic Sea (including its catchment area) is positive and the excess water masses flow via the Skagerrak into the Atlantic Ocean. The surplus of precipitation leads to the positive dex signal in the Baltic Sea. A similar feature is detected for the Arctic Ocean.

To evaluate the simulated global distribution of dex in precipitation and ocean surface waters, we use again the GNIP and GISS data sets. The plotted station values in Fig. 6c and e do not show a systematic regional bias of the modelled dex signal in precipitation (Fig. 6c) or ocean surface waters (Fig. 6e). We note that some of the measured dex values, e.g. a series of GISS data points in the Southern Indian Ocean, show strong small-scale variations that cannot be matched due to the coarse horizontal model resolution. However, even on a large-scale average the model results tend to un-

## Glacial–interglacial changes of H<sub>2</sub><sup>18</sup>O, HDO and deuterium excess

M. Werner et al.

Title Page

Abstract

Introduction

Conclusions

References

Tables

Figures

◀

▶

◀

▶

Back

Close

Full Screen / Esc

Printer-friendly Version

Interactive Discussion



derestimate the dex values in precipitation with a RMSE of 2.9‰ while the simulated dex values of ocean surface waters are in general higher (RMSE: 1.8‰) than measurements listed in the GISS database. This combination of underestimation (overestimation) of simulated dex values in precipitation (ocean surface waters) might indicate that the general description of fractionation processes during the evaporation of ocean surface waters, implemented as proposed by Merlivat and Jouzel (1979), should be revised and refined. This finding is in agreement with recent studies by Steen-Larsen et al. (2014b, a; 2015), which reveal substantial deviations of the simulated dex signal in water vapour in Greenland, Bermuda, and Iceland, by several atmosphere GCM as compared to laser-based spectroscopy measurements of isotopes in water vapour.

## 4.2 Changes of the last glacial maximum

### 4.2.1 Land surface temperature and precipitation changes

Due to the prescribed changed glacial ice sheet configuration, changed orbital parameters and changed greenhouse gas concentrations the simulated LGM climate on glacier-free terrestrial areas is on average  $-5.9^{\circ}\text{C}$  colder than the modeled PI climate. Most regions show a rather uniform cooling in the range of  $-4$  to  $-8^{\circ}\text{C}$  (Fig. 7a). Exceptionally cold regions are mostly adjacent to the prescribed Laurentide and Fennoscandian ice sheet, e.g. part of central North America and central Europe. Another region of exceptional cooling is a large part of Siberia with a cooling of down to  $-15^{\circ}\text{C}$ . The only region with a distinct above-average warming is located at Alaska. This region most likely warmed during the LGM due to the increased distance to sea ice-covered Arctic ocean regions, caused by the glacial sea-level drop of approx. 120 m. Our results are in overall agreement with the ensemble-mean LGM changes in temperature by the fully coupled climate simulations performed within the PMIP2 and CMIP5/PMIP3 projects (not shown; Braconnot et al., 2007; Harrison et al., 2014). These simulations also indicate for the LGM a maximum cooling of surface temperature over the ice sheets by

Title Page

Abstract

Introduction

Conclusions

References

Tables

Figures



Back

Close

Full Screen / Esc

Printer-friendly Version

Interactive Discussion



**Glacial–interglacial  
changes of H<sub>2</sub><sup>18</sup>O,  
HDO and deuterium  
excess**

M. Werner et al.

Title Page

Abstract

Introduction

Conclusions

References

Tables

Figures



Back

Close

Full Screen / Esc

Printer-friendly Version

Interactive Discussion

about  $-30^{\circ}$  and an average cooling of glacier-free land surfaces between  $-2$  and  $-5^{\circ}\text{C}$ , except for a colder-than-average Siberian region.

For a comparison with proxy data we compare our model results to the LGM continental temperature and precipitation reconstruction by Bartlein et al. (2011). This reconstruction is mainly based on subfossil pollen and plant macrofossil data. For the 81 sites contained in the temperature dataset of Bartlein et al., the simulated annual mean LGM temperature change is in 24 cases (22 cases) more than  $2^{\circ}\text{C}$  warmer (colder) than the reconstructed temperature change (Fig. 7b). While the model-data deviations of LGM warming anomalies range between  $+0$  and  $+20^{\circ}\text{C}$ , the anomalies of LGM cooling are underestimated by down to  $-15^{\circ}\text{C}$ . Several sites with the largest model-data deviations are located near the border of the prescribed Laurentide and Fennoscandinavian ice sheets. These deviations might simply be caused by the rather coarse model resolution of  $3.8^{\circ} \times 3.8^{\circ}$ , which cannot resolve small-scale temperature changes close to the prescribed glacier area in sufficient detail.

Simulated LGM precipitation changes (Fig. 7c) show a drying of large parts of Siberia and North America, and smaller parts of South America, Africa and East Asia. A wetting is found for the region of California, western Europe, the Brazilian Highlands, South Africa and most parts of Australia. Especially the regions of a wetter LGM climate strongly deviate from older PMIP2 simulations (Braconnot et al., 2007) but are in good overall agreement with the latest CMIP5 LGM experiments (Harrison et al., 2014). A comparison of the simulation results with the precipitation reconstruction by Bartlein et al. (2011) reveals less agreement between simulated and reconstructed precipitation (Fig. 7c and d). In agreement with the reconstructions, the model simulates a drying over vast parts of Northern Eurasia and Siberia, as well as dipole pattern of wetter (drier) conditions south of the margin of the Laurentide ice sheet in western (eastern) North America. However, the model fails to simulate a drying of Western and Central Europe during the LGM, as indicated by fossil plant data. Overall, the amplitude of modelled changes in the hydrological cycle ( $-490$  to  $+250\text{ mm yr}^{-1}$ ) is weaker than the range of the reconstructed changes ( $-1240$  to  $+720\text{ mm yr}^{-1}$ ), and the gen-

eral underestimation of LGM dryness is in line with model results from the PMIP2 and CMIP5/PMIP3 projects (Harrison et al., 2014).

#### 4.2.2 LGM changes of $\delta^{18}\text{O}$ in precipitation

Previous studies have already shown that the colder climate of the LGM leads to generally more depleted  $\delta^{18}\text{O}_p$  values in precipitation (Lee et al., 2008; Risi et al., 2010b). This depletion is a direct consequence of the changed (temperature-dependent) fractionation strength during both evaporation and condensation processes. Over glacier-free land surfaces, we calculate a precipitation-weighted mean decrease of  $\delta^{18}\text{O}_p$  in precipitation by  $-0.24\text{‰}$ . For tropical and sub-tropical regions in Mid- and South America, Africa, Australia, and parts of Asia, our simulation reveals almost no LGM-PI changes in  $\delta^{18}\text{O}_p$  in precipitation (Fig. 8a). Glacial changes of down to  $-3\text{‰}$  occur in precipitation over the southern parts of South America and Africa, the Tibetan Plateau, as well as over major parts of Siberia, North America, and Alaska. The strongest simulated LGM-PI changes of  $\delta^{18}\text{O}_p$  in precipitation (down to  $-12\text{‰}$ ) are found over the glacier areas of both the Northern and Southern Hemisphere. We restrict a first quantitative evaluation of the simulated LGM-PI  $\delta^{18}\text{O}_p$  anomalies in precipitation to the chosen data of 21 ice cores (Table 1) and 8 speleothem records (Table 2). Our dataset is partly identical to the one used by Risi et al. (2010b) and by Brennan et al. (2012) and enables a direct comparison with these previous model studies. For the speleothem records, we use both the simulated LGM-PI temperature and  $\delta^{18}\text{O}_p$  changes to compare the model results with the reconstructions. Overall, the model results agree well ( $r^2 = 0.64$ , RMSE =  $2.8\text{‰}$ ) with the reconstructed LGM-PI  $\delta^{18}\text{O}_p$  changes at the various sites (Fig. 8b). The largest deviations are found for the Camp Century ice core (measured LGM-PI  $\delta^{18}\text{O}_p$  difference:  $-12.9\text{‰}$ , modelled:  $-9.4\text{‰}$ ) and for the  $\delta^{18}\text{O}_p$  in precipitation at 4 out of 5 tropical ice core locations.

From the simulated LGM-PI temperature and  $\delta^{18}\text{O}_p$  changes we calculate the temporal  $\delta^{18}\text{O}_p$ - $T$  gradient  $m$  in a specific grid box as  $m = (\delta^{18}\text{O}_{p,\text{LGM}} - \delta^{18}\text{O}_{p,\text{PI}}) / (T_{\text{LGM}} -$

### Glacial–interglacial changes of $\text{H}_2^{18}\text{O}$ , HDO and deuterium excess

M. Werner et al.

Title Page

Abstract

Introduction

Conclusions

References

Tables

Figures



Back

Close

Full Screen / Esc

Printer-friendly Version

Interactive Discussion





$T_{PI}$ ), with  $T$  as the surface temperature at the precipitation site. We restrict our calculation to mid- and high-latitude regions with an annual mean PI temperature  $T_{PI}$  below  $+20^{\circ}\text{C}$ . As a further selection criteria, we use grid cells with a simulated LGM-PI cooling of at least  $-2^{\circ}\text{C}$ , only. The calculated temporal  $\delta^{18}\text{O}_p-T$  gradient  $m$  for the selected grid cells ( $N = 1195$ ) ranges between  $-0.53$  and  $+0.85$  (Fig. 8c). For only 17 % of the grid cells ( $N = 198$ ), the calculated temporal  $\delta^{18}\text{O}_p-T$  gradient ranges between  $+0.5$  and  $+0.7\text{‰}\text{C}^{-1}$ , close to the simulated modern spatial  $\delta^{18}\text{O}_p-T$  gradient of  $m = 0.58\text{‰}\text{C}^{-1}$  (see Chapter 4.1.1). In a vast majority of the grid cells (80 %), the temporal  $\delta^{18}\text{O}_p-T$  gradient is below the modern spatial one, while a higher temporal gradient is simulated for 3 % of the selected cells, only. A clear difference between temporal and spatial  $\delta^{18}\text{O}_p-T$  gradient has already been reported for Greenland (Buizert et al., 2014; Jouzel, 1999; Werner et al., 2000) and might be caused by different mechanisms (e.g., change in precipitation seasonality, shift of water vapour source regions and transport pathways, varying vertical temperature gradients and atmospheric heights of precipitation formation). However, our results indicate that such a potential bias of the  $\delta^{18}\text{O}_p$ -thermometer (if a modern spatial  $\delta^{18}\text{O}_p-T$  gradient is used for past temperature reconstructions) might not exist for Greenland, only, but also for large parts of the mid- and high-latitude regions. The robustness and implications of these findings will be further investigated in future studies.

Next, we take a more detailed look at the simulation results over both polar ice caps. For the compilation of ice core data listed in Table 1, our model results are in good agreement with glacial  $\delta^{18}\text{O}_p$  anomalies found in Antarctic ice cores (Fig. 9). Mean model-data deviation is 1.1 % with the largest mismatch for the Byrd ice core (2.3 %). For Greenland, model-data differences are slightly higher than for Antarctica as the model underestimates the LGM-PI  $\delta^{18}\text{O}_p$  changes by 1.5 %, on average. As already noted above, the largest mismatch is found for the Camp Century ice core (3.5 %). The reason for this stronger model-data mismatch for Greenland as compared to Antarctica could be partly due to the coarse model resolution, or caused by an erroneous warm bias of SST in the source regions of vapour transported to Greenland. Testing

## Glacial–interglacial changes of $\text{H}_2^{18}\text{O}$ , HDO and deuterium excess

M. Werner et al.

[Title Page](#)[Abstract](#)[Introduction](#)[Conclusions](#)[References](#)[Tables](#)[Figures](#)[⏪](#)[⏩](#)[◀](#)[▶](#)[Back](#)[Close](#)[Full Screen / Esc](#)[Printer-friendly Version](#)[Interactive Discussion](#)

and evaluating these different hypotheses will require further coupled simulations and analyses.

### 4.2.3 LGM changes of ocean temperatures and marine $\delta^{18}\text{O}$ signals

The state of the glacial oceans has been under debate since the first reconstruction of global LGM sea surface temperatures (SST) and sea ice coverage by the CLIMAP group (CLIMAP Project Members, 1976). As compared to CLIMAP, the most recent SST reconstruction by the MARGO project (MARGO Project Members, 2009) indicates, among others, a more pronounced cooling in the eastern mid-latitude North Atlantic than in the western basin, ice-free conditions in the Nordic seas during glacial summer, as well as a 1–3 °C cooling of the western Pacific warm pool. The study also revealed the presence of large longitudinal gradients in LGM SST anomalies in all the ocean basins, which are absent in the majority of atmosphere–ocean coupled simulations of the PMIP2 project (MARGO Project Members, 2009).

The physical state of the glacial ocean of our LGM simulation has already been analysed and described in detail by Zhang et al. (2013). In agreement with this previous study, we also find a rather uniform SST cooling in the range of 2–4 °C during the LGM in our simulation, comparable to the results of several atmosphere–ocean GCM participating in PMIP2 and CMIP5/PMIP3 (Zhuang and Giardino, 2012). For the isotopic composition of ocean surface waters  $\delta^{18}\text{O}_{\text{Oce}}$ , we simulate a globally averaged mean increase of +0.84 ‰ as compared to the PI ocean state. This is noteworthy, as we adjusted in our LGM simulation the global ocean isotopic composition by +1 ‰ to account for the change in global ice volume. A less-than-average part of this increase (0.94 ‰) is found in surface and shallow water depth down to approx. 1000 m, while deeper water masses show a glacial increase of up to +1.06 ‰ in our simulation. In addition, the simulated glacial increase is not spatially uniform for the ocean surface waters, neither. For most regions the LGM anomalies are in the order of +0.5 to +1 ‰ (Fig. 10a), but more positive LGM  $\delta^{18}\text{O}_{\text{Oce}}$  anomalies exist in the ACC region (up to

## Glacial–interglacial changes of $\text{H}_2^{18}\text{O}$ , HDO and deuterium excess

M. Werner et al.

Title Page

Abstract

Introduction

Conclusions

References

Tables

Figures



Back

Close

Full Screen / Esc

Printer-friendly Version

Interactive Discussion



+1.5‰), the Mediterranean region (up to +3‰), as well as in the North Atlantic region above approx. 30° N (up to +2.3‰).

As both water temperatures and  $\delta^{18}\text{O}_{\text{occe}}$  are explicitly simulated by our model setup, we can calculate  $\delta^{18}\text{O}_{\text{C(PDB)}}$  for the PI and LGM simulation and then compare our model results to the marine calcite  $\delta^{18}\text{O}_{\text{C}}$  dataset documented by Caley et al. (2014). In agreement with the simulated pattern of LGM  $\delta^{18}\text{O}_{\text{occe}}$  anomalies in seawater, the simulated  $\delta^{18}\text{O}_{\text{C}}$  changes in calcite are strongest in the ACC region, the Mediterranean Sea and the North Atlantic. Positive  $\delta^{18}\text{O}_{\text{C}}$  anomalies reach maximum values of +2.6‰ in the North Atlantic. Comparing the pattern of simulated LGM-PI changes of  $\delta^{18}\text{O}_{\text{occe}}$  in surface waters (Fig. 10a) and  $\delta^{18}\text{O}_{\text{C}}$  in calcite (Fig. 10b) it is also noteworthy that (a) there exists an additional strong positive LGM  $\delta^{18}\text{O}_{\text{C}}$  anomaly in the East China Sea and parts of the North Pacific, which has no counterpart in the  $\delta^{18}\text{O}_{\text{occe}}$  changes of ocean surface waters, (b) the  $\delta^{18}\text{O}_{\text{C}}$  anomalies in the Pacific ACC region are shifted northwards by approx. 5° as compared to the  $\delta^{18}\text{O}_{\text{occe}}$  surface waters anomalies.

A comparison of the simulated  $\delta^{18}\text{O}_{\text{C}}$  values in ocean surface waters between 0–50 m to the  $\delta^{18}\text{O}_{\text{C}}$  data set of planktic LGM  $\delta^{18}\text{O}_{\text{C}}$  anomalies compiled by Caley et al. (2014) shows a systematic overestimation of simulated LGM  $\delta^{18}\text{O}_{\text{C}}$  changes for the Mediterranean Sea (Fig. 10c), only. For all three major oceans, our model simulation both underestimates and overestimates LGM  $\delta^{18}\text{O}_{\text{C}}$  changes at various marine sediment sites. Model-data differences are mostly within the order of the reported uncertainty of the reconstructed LGM  $\delta^{18}\text{O}_{\text{C}}$  anomalies, as reported by Caley et al. (2014). The simulated spatial pattern of LGM  $\delta^{18}\text{O}_{\text{C}}$  anomalies in surface waters shows some remarkable resemblance to the model results of Caley et al. (2014) using the iLOVECLIM model. In their study, Caley et al. also find the strongest positive  $\delta^{18}\text{O}_{\text{C}}$  anomalies in the North Atlantic, parts of the northern Pacific as well as in the ACC. In contrast to our simulation, Caley et al. report an additional strong  $\delta^{18}\text{O}_{\text{C}}$  anomaly in the northern Indian Ocean.

## GMDD

8, 8835–8894, 2015

### Glacial–interglacial changes of $\text{H}_2^{18}\text{O}$ , HDO and deuterium excess

M. Werner et al.

Title Page

Abstract

Introduction

Conclusions

References

Tables

Figures



Back

Close

Full Screen / Esc

Printer-friendly Version

Interactive Discussion



In Fig. 11 mean LGM-PI changes of  $\delta^{18}\text{O}_c$  for the Atlantic cross section (60–0° W) and the Pacific cross section (150° E to 110° W) are shown. For both oceans, model results show the strongest positive change of  $\delta^{18}\text{O}_c$  between 500 and 3000 m. While  $\delta^{18}\text{O}_c$  changes of up to +2.6‰ are simulated at around 30° N for the Atlantic basin, the  $\delta^{18}\text{O}_c$  changes in the Pacific water masses are in general lower (up to +2.2‰) and the region of the largest change is located between 0 and 50° S. The available benthic foraminifera data compiled by Caley et al. (2014) partly supports these findings. The too positive modelled  $\delta^{18}\text{O}_c$  values in the North Atlantic in a depth between approx. 2500 and 4000 m indicate that the simulated NADW formation is probably too strong and too deep. By combining a series of isotope studies with different NADW strengths with available proxy studies of the glacial NADW formation (Duplessy et al., 1980) it should be possible to constrain and improve this aspect of the isotope-enhanced version of the ECHAM5/MPI-OM model. Recently, Roche et al. (2014) presented a similar approach for an improved modelling of Heinrich event 1. However, performing such a set of fully coupled sensitivity experiments is computationally demanding and beyond the scope of this paper.

#### 4.2.4 Glacial changes of the deuterium excess

In Fig. 12a, we show the global pattern of simulated LGM-PI dex anomalies in precipitation over land surfaces. Changes are rather minor, in the order of –3 to +3‰, except for a clear positive anomaly (up to +6‰) in North America south-west of the Laurentide ice sheet margin, and strong negative anomalies (down to –7‰) above Greenland and Antarctica. For ocean surface waters, the simulated dex anomalies are even smaller and almost everywhere in the range of  $\pm 1$ ‰ (not shown). Figure 12b shows the simulated LGM-PI dex anomalies in water vapour of the lowest atmospheric model layer above the ocean surface (discussed below).

So far, ice cores are the only paleoproxy archive, which allow for reconstructing past changes of deuterium excess values in precipitation. In Fig. 13 we compare our model

5 results of annual mean dex changes in precipitation between the LGM and PI simulation with the compiled ice core data (Table 2). Mean absolute deviation between modelled LGM-PI anomalies and ice core data from Antarctica is 1.6 ‰. For Greenland ice cores, LGM dex values have been only reported for the GRIP ice core, so far. Here, model results underestimate the LGM-PI dex change by 2 ‰. The overall good agreement between measured and modelled LGM dex changes is remarkable, as isotope-enabled GCM have had some difficulties simulating the measured LGM dex changes in Antarctic ice cores, so far (e.g., Risi et al., 2010b; Werner et al., 2001). As dex values in polar ice cores depend on climate condition during evaporation of the source water, and as the SST of our simulation are more uniform and lower than the latest MARGO reconstruction, one may ask if the good dex agreement is due to the modelled SST. For testing this hypothesis we have conducted an atmosphere-only ECHAM5-wiso simulation with identical LGM boundary conditions as for the fully coupled ECHAM5/MPI-OM setup but using the GLAMAP LGM SST reconstruction, which was supplemented by older CLIMAP data in order to have global coverage (Schäfer-Neth and Paul, 2003a, b). For  $\delta^{18}\text{O}_{\text{oce}}$  ( $\delta\text{D}_{\text{oce}}$ ), we prescribed a uniform glacial increase of +1 ‰ (+8 ‰) in this simulation. In this ECHAM5-wiso sensitivity study, the relatively warm (sub)tropical GLAMAP SST reconstruction leads to smaller simulated negative dex anomalies, or even slightly positive dex anomalies for Vostok and Dome F (Fig. 13). The RMSE of all Antarctic ice cores is 2.3 ‰, which is 0.7 ‰ worse than in the fully-coupled simulation. We are aware that such a comparison of the fully coupled ECHAM5/MPI-OM setup with an atmosphere-only ECHAM5 experiment with prescribed SST might be hampered by neglecting any atmosphere–ocean feedback in the later. Nevertheless, our simulations indicate that glacial SST, which are cooler than the GLAMAP reconstruction, lead to an improved simulation of dex changes, at least over Antarctica. However, for Greenland the simulated dex anomaly at the GRIP drilling site becomes too low in our fully coupled simulation. But as no more LGM-PI dex records of Greenland ice core records have been published, yet, it remains an open question if this deviation points to a systematic bias in our simulation. More LGM-PI dex data from polar ice cores in combination with

## Glacial–interglacial changes of $\text{H}_2^{18}\text{O}$ , HDO and deuterium excess

M. Werner et al.

[Title Page](#)[Abstract](#)[Introduction](#)[Conclusions](#)[References](#)[Tables](#)[Figures](#)[Back](#)[Close](#)[Full Screen / Esc](#)[Printer-friendly Version](#)[Interactive Discussion](#)

further isotope simulations are required to put an additional, highly valuable constrain on available LGM SST reconstructions.

Pfahl and Soedemann (2014) suggest in their study that the typical interpretation of dex variations in ice core records as SST changes might have to be adapted to reflect climatic influences on relative humidity during evaporation. To test this hypothesis, we look at the simulated LGM-PI dex anomalies in water vapour of the lowest atmospheric layer, directly above the ocean surface (Fig. 12b). It is safe to assume that most water transported to Antarctica will stem from Southern Hemisphere marine vapour source regions, and not from continental vapour sources. Simulated LGM-PI dex anomalies of the vapour vary between 0 and  $-5\%$  for most ocean regions with a clear gradient towards more negative dex values in the higher latitudinal regions. Plotting these simulated changes of dex in vapour against the modelled relative humidity change between LGM and PI over the ocean surface reveals no correlation between these humidity changes and the simulated dex variations in the vapour layer. As seen in Fig. 14a, simulated LGM values of the relative humidity of the vapour layer above ocean surface varies just by  $\pm 5\%$  as compared to the PI values. In contrast, modelled LGM SST changes of the Southern Hemisphere cover a range of 0 to  $-15^\circ\text{C}$ , and a strong correlation ( $r^2 = 0.78$ ) between simulated glacial SST changes and LGM dex anomalies in the vapour above the ocean surface is found (Fig. 14b). We rate this finding as a support of the “classical” interpretation of dex changes in Antarctic ice cores as a proxy for SST changes in the source regions of water transported to Antarctica. However we are aware that several recent studies of dex in water vapour have revealed a large bias between measurements and simulations by different isotope-enabled atmospheric GCM (Steen-Larsen et al., 2014b, 2015). We cannot resolve this conundrum with the performed simulations and will investigate this topic in more detail in the future.

## GMDD

8, 8835–8894, 2015

### Glacial–interglacial changes of $\text{H}_2^{18}\text{O}$ , HDO and deuterium excess

M. Werner et al.

Title Page

Abstract

Introduction

Conclusions

References

Tables

Figures

◀

▶

◀

▶

Back

Close

Full Screen / Esc

Printer-friendly Version

Interactive Discussion



## 5 Summary and conclusions

In this study we present the first simulations of the fully coupled Earth System Model ECHAM5/MPI-OM. The model has been enhanced by an explicit stable water isotope diagnostics in all relevant model components: atmosphere, land surface, terrestrial discharge, and ocean. The hydrological cycle and its isotopic balance are fully closed in the model setup, and the model has been run successfully into equilibrium under PI and LGM boundary conditions.

First-order isotope variations in precipitation ( $\delta^{18}\text{O}_p$ ,  $\delta\text{D}_p$ ) for the PI and LGM climate are in good to very good agreement with available present-day observations from the GNIP database, and with LGM isotope data from various ice core and speleothem records. The largest  $\delta$ -deviations between present-day observations and model results are found in high-latitude regions and are caused by a warm bias of the coupled model, similar to the reported error of the atmosphere-only GCM ECHAM5-wiso (Werner et al., 2011). Such a warm bias, especially over Antarctica, is frequent in GCM (Masson-Delmotte et al., 2006) and is partly related to the coarse spatial resolution of our model setup.

The simulated modern spatial  $\delta$ - $T$  relation is also in good agreement with the observed one, based on a selection of GNIP and ice core data. A first assessment of the stability of this relation for LGM-PI climate changes reveals that the temporal  $\delta$ - $T$  gradient might have been substantially lower than the modern spatial one for most mid- to high-latitude regions. Such a deviation, which causes a strong bias in the “classical”  $\delta$ -paleothermometry approach, is known for Greenland ice cores (Jouzel, 1999) but has not been discussed for other Northern Hemisphere regions, so far. Future in-depth analyses of our model results can help to achieve an improved interpretation of available isotope records, e.g. from speleothems or permafrost ice wedges (Meyer et al., 2015), from these regions.

For the PI climate, simulated marine  $\delta^{18}\text{O}_{\text{oce}}$  values broadly fit to available measurements compiled in the GISS database. For the Atlantic, Pacific, and Indian Ocean the

GMDD

8, 8835–8894, 2015

### Glacial–interglacial changes of $\text{H}_2^{18}\text{O}$ , HDO and deuterium excess

M. Werner et al.

Title Page

Abstract

Introduction

Conclusions

References

Tables

Figures

⏪

⏩

◀

▶

Back

Close

Full Screen / Esc

Printer-friendly Version

Interactive Discussion



## Glacial–interglacial changes of $\text{H}_2^{18}\text{O}$ , HDO and deuterium excess

M. Werner et al.

Title Page

Abstract

Introduction

Conclusions

References

Tables

Figures

⏪

⏩

◀

▶

Back

Close

Full Screen / Esc

Printer-friendly Version

Interactive Discussion

largest model-data deviations in ocean surface waters are found in the vicinity of large river estuaries, the Sea of Okhotsk, parts of the Bering Sea, and the Baltic Sea. Like for the model deficits in  $\delta^{18}\text{O}_p$ , these deviations are most likely related to the rather coarse resolution of the ocean model component MPI-OM, which hampers a realistic simulation of water mass mixing in these coastal regions. For the Arctic, modelled  $\delta^{18}\text{O}_{\text{oce}}$  values in surface waters show a more general negative bias as compared to the GISS data. It remains an open question if this bias can also be simply related to an inadequate mixing of the isotopically depleted inflow of Arctic rivers into this ocean basin, or if a more general model bias in the hydrological balance of the Arctic Ocean exists. For the simulated LGM  $\delta^{18}\text{O}$  changes, a comparison of model results with available  $\delta^{18}\text{O}_c$  calcite data from planktic and benthic foraminifera shells reveals a partly model-data match, only. For the North Atlantic, the modelled glacial NADW formation appears too deep and too strong in our LGM simulation. However, more sensitivity studies are necessary to better constrain this aspect of glacial ocean circulation change. As a next step, we will also more explicitly simulate the dependence of  $\delta^{18}\text{O}_c$  on the surrounding water conditions, and analyse the stability of the relation between  $\delta^{18}\text{O}$  and salinity in ocean waters under the different climate conditions.

The simulation results for second-order changes of  $\delta^{18}\text{O}$  and  $\delta\text{D}$  are also satisfactory. In our analyses, an overall good fit of modern deuterium excess values in precipitation and ocean surface waters with the available observations is found. However, on large-scale average the ECHAM5/MPI-OM isotope results tend to slightly underestimate the dex values in precipitation and, at the same time, overestimate the simulated dex values of ocean surface waters. This combination of opposite biases suggests that the implementation of fractionation processes during the evaporation of ocean surface waters in our model setup, which is strictly following the approach by Merlivat and Jouzel (1979), should maybe be revised and refined in future studies. For LGM-PI changes of deuterium excess, only measurements from Greenland and Antarctic ice cores are available, at present. Our simulation results indicate that LGM Southern Hemisphere SST, which are cooler than the CLIMAP reconstruction, lead to



an improved simulation of dex values in Antarctic precipitation. In addition, our analyses reveal that modelled glacial dex changes are strongly correlated to LGM-PI SST changes, but not to relative humidity changes in the evaporation regions.

In this study we have presented first results of the newly developed isotope-enabled version of the Earth System Model ECHAM5/MPI-OM. We have focused on two equilibrium simulations under the pre-industrial and last glacial maximum period, only, due to their different climate states and the wealth of available observational data from both periods. Future studies will investigate changes in the hydrological cycle and its isotopic composition for further climate periods of the past, e.g. the last interglacial, as well as for the transition between them.

## References

- Baertschi, P.: Absolute  $^{18}\text{O}$  content of standard mean ocean water, *Earth Planet. Sc. Lett.*, 31, 341–344, doi:10.1016/0012-821X(76)90115-1, 1976.
- Bartlein, P. J., Harrison, S. P., Brewer, S., Connor, S., Davis, B. A. S., Gajewski, K., Guiot, J., Harrison-Prentice, T. I., Henderson, A., Peyron, O., Prentice, I. C., Scholze, M., Seppä, H., Shuman, B., Sugita, S., Thompson, R. S., Viau, A. E., Williams, J., and Wu, H.: Pollen-based continental climate reconstructions at 6 and 21 ka: a global synthesis, *Clim. Dynam.*, 37, 775–802, doi:10.1007/s00382-010-0904-1, 2011.
- Bigg, G. R. and Rohling, E. J.: An oxygen isotope data set for marine waters, *J. Geophys. Res.-Oceans*, 105, 8527–8535, 2000.
- Bonne, J.-L., Masson-Delmotte, V., Cattani, O., Delmotte, M., Risi, C., Sodemann, H., and Steen-Larsen, H. C.: The isotopic composition of water vapour and precipitation in Ivittuut, southern Greenland, *Atmos. Chem. Phys.*, 14, 4419–4439, doi:10.5194/acp-14-4419-2014, 2014.
- Braconnot, P., Otto-Bliesner, B., Harrison, S., Joussaume, S., Peterchmitt, J.-Y., Abe-Ouchi, A., Crucifix, M., Driesschaert, E., Fichefet, Th., Hewitt, C. D., Kageyama, M., Kitoh, A., Laîné, A., Loutre, M.-F., Marti, O., Merkel, U., Ramstein, G., Valdes, P., Weber, S. L., Yu, Y., and Zhao, Y.: Results of PMIP2 coupled simulations of the Mid-Holocene and Last Glacial Maxi-

**GMDD**

8, 8835–8894, 2015

## Glacial–interglacial changes of $\text{H}_2^{18}\text{O}$ , HDO and deuterium excess

M. Werner et al.

Title Page

Abstract

Introduction

Conclusions

References

Tables

Figures

◀

▶

◀

▶

Back

Close

Full Screen / Esc

Printer-friendly Version

Interactive Discussion



## Glacial–interglacial changes of H<sub>2</sub><sup>18</sup>O, HDO and deuterium excess

M. Werner et al.

Title Page

Abstract

Introduction

Conclusions

References

Tables

Figures

◀

▶

◀

▶

Back

Close

Full Screen / Esc

Printer-friendly Version

Interactive Discussion

3000 – Part 1: experiments and large-scale features, *Clim. Past*, 3, 261–277, doi:10.5194/cp-3-261-2007, 2007.

Brennan, C. E., Weaver, A. J., Eby, M., and Meissner, K. J.: Modelling oxygen isotopes in the University of Victoria Earth system climate model for pre-industrial and last glacial maximum conditions, *Atmos. Ocean*, 50, 447–465, doi:10.1080/07055900.2012.707611, 2012.

Broecker, W. S., Peng, T. H., Jouzel, J., and Russell, G.: The magnitude of global fresh-water transports of importance to ocean circulation, *Clim. Dynam.*, 4, 73–79, doi:10.1007/BF00208902, 1990.

Brovkin, V., Raddatz, T., Reick, C. H., Claussen, M., and Gayler, V.: Global biogeophysical interactions between forest and climate, *Geophys. Res. Lett.*, 36, L07405, doi:10.1029/2009gl037543, 2009.

Buizert, C., Gkinis, V., Severinghaus, J. P., He, F., Lecavalier, B. S., Kindler, P., Leuenberger, M., Carlson, A. E., Vinther, B., Masson-Delmotte, V., White, J. W. C., Liu, Z., Otto-Bliesner, B., and Brook, E. J.: Greenland temperature response to climate forcing during the last deglaciation, *Science*, 345, 1177–1180, 2014.

Caley, T., Roche, D. M., Waelbroeck, C., and Michel, E.: Oxygen stable isotopes during the Last Glacial Maximum climate: perspectives from data–model (iLOVECLIM) comparison, *Clim. Past*, 10, 1939–1955, doi:10.5194/cp-10-1939-2014, 2014.

CLIMAP Project Members: Surface of Ice-Age Earth, *Science*, 191, 1131–1137, 1976.

Coplen, T. B.: Normalization of oxygen and hydrogen isotope data, *Chem. Geol.*, 72, 293–297, doi:10.1016/0168-9622(88)90042-5, 1988.

Craig, H. and Gordon, L. I.: Deuterium and oxygen 18 variations in the ocean and the marine atmosphere, edited by: Tongiogi, E., Consiglio nazionale delle ricerche, Laboratorio de geologia nucleare, Spoleto, Italy, 9–130, 1965.

Cruz, F. W., Burns, S. J., Karmann, I., Sharp, W. D., Vuille, M., Cardoso, A. O., Ferrari, J. A., Dias, P. L. S., and Viana, O.: Insolation-driven changes in atmospheric circulation over the past 116,000 years in subtropical Brazil, *Nature*, 434, 63–66, doi:10.1038/Nature03365, 2005.

Dansgaard, W.: Stable isotopes in precipitation, *Tellus*, 16, 436–468, 1964.

Dansgaard, W., Johnsen, S. J., Møller, J., and Langway, C. C.: One thousand centuries of climatic record from Camp Century on the Greenland ice sheet, *Science*, 166, 377–380, doi:10.1126/science.166.3903.377, 1969.

## Glacial–interglacial changes of H<sub>2</sub><sup>18</sup>O, HDO and deuterium excess

M. Werner et al.

Title Page

Abstract

Introduction

Conclusions

References

Tables

Figures

◀

▶

◀

▶

Back

Close

Full Screen / Esc

Printer-friendly Version

Interactive Discussion



de Wit, J. C., van der Straaten, C. M., and Mook, W. G.: Determination of the absolute hydrogen isotopic ratio of V-SMOW and SLAP, *Geostandard. Newslett.*, 4, 33–36, doi:10.1111/j.1751-908X.1980.tb00270.x, 1980.

Dee, D. P., Uppala, S. M., Simmons, A. J., Berrisford, P., Poli, P., Kobayashi, S., Andrae, U., Balmaseda, M. A., Balsamo, G., Bauer, P., Bechtold, P., Beljaars, A. C. M., van de Berg, L., Bidlot, J., Bormann, N., Delsol, C., Dragani, R., Fuentes, M., Geer, A. J., Haimberger, L., Healy, S. B., Hersbach, H., Holm, E. V., Isaksen, L., Kallberg, P., Kohler, M., Matricardi, M., McNally, A. P., Monge-Sanz, B. M., Morcrette, J. J., Park, B. K., Peubey, C., de Rosnay, P., Tavolato, C., Thepaut, J. N., and Vitart, F.: The ERA-Interim reanalysis: configuration and performance of the data assimilation system, *Q. J. Roy. Meteor. Soc.*, 137, 553–597, doi:10.1002/Qj.828, 2011.

Delaygue, G., Jouzel, J., and Dutay, J. C.: Oxygen 18-salinity relationship simulated by an oceanic general circulation model, *Earth Planet. Sc. Lett.*, 178, 113–123, doi:10.1016/S0012-821X(00)00073-X, 2000.

Dodd, P. A., Rabe, B., Hansen, E., Falck, E., Mackensen, A., Rohling, E., Stedmon, C., and Kristiansen, S.: The freshwater composition of the Fram Strait outflow derived from a decade of tracer measurements, *J. Geophys. Res.*, 117, C11005, doi:10.1029/2012JC008011, 2012.

Dreybrodt, W. and Scholz, D.: Climatic dependence of stable carbon and oxygen isotope signals recorded in speleothems: from soil water to speleothem calcite, *Geochim. Cosmochim. Ac.*, 75, 734–752, doi:10.1016/j.gca.2010.11.002, 2011.

Duplessy, J. C., Moyes, J., and Pujol, C.: Deep-water formation in the North-Atlantic Ocean during the last Ice-Age, *Nature*, 286, 479–482, 1980.

Fleitmann, D., Burns, S. J., Mudelsee, M., Neff, U., Kramers, J., Mangini, A., and Matter, A.: Holocene forcing of the Indian Monsoon recorded in a stalagmite from Southern Oman, *Science*, 300, 1737–1739, doi:10.1126/science.1083130, 2003.

Haese, B., Werner, M., and Lohmann, G.: Stable water isotopes in the coupled atmosphere–land surface model ECHAM5-JSBACH, *Geosci. Model Dev.*, 6, 1463–1480, doi:10.5194/gmd-6-1463-2013, 2013.

Hagemann, S. and Gates, L. D.: Improving a subgrid runoff parameterization scheme for climate models by the use of high resolution data derived from satellite observations, *Clim. Dynam.*, 21, 349–359, doi:10.1007/s00382-003-0349-x, 2003.

## Glacial–interglacial changes of H<sub>2</sub><sup>18</sup>O, HDO and deuterium excess

M. Werner et al.

Title Page

Abstract

Introduction

Conclusions

References

Tables

Figures



Back

Close

Full Screen / Esc

Printer-friendly Version

Interactive Discussion



Harrison, S. P., Bartlein, P. J., Brewer, S., Prentice, I. C., Boyd, M., Hessler, I., Holmgren, K., Izumi, K., and Willis, K.: Climate model benchmarking with glacial and mid-Holocene climates, *Clim. Dynam.*, 43, 671–688, doi:10.1007/s00382-013-1922-6, 2014.

Hibler, W. D.: A dynamic thermodynamic sea ice model, *J. Phys. Oceanogr.*, 9, 815–846, 1979.

Hoffmann, G., Werner, M., and Heimann, M.: Water isotope module of the ECHAM atmospheric general circulation model: a study on timescales from days to several years, *J. Geophys. Res.-Atmos.*, 103, 16871–16896, 1998.

Hoffmann, G., Ramirez, E., Taupin, J. D., Francou, B., Ribstein, P., Delmas, R., Durr, H., Gallaire, R., Simoes, J., Schotterer, U., Stiévenard, M., and Werner, M.: Coherent isotope history of Andean ice cores over the last century, *Geophys. Res. Lett.*, 30, 1179, doi:10.1029/2002gl014870, 2003.

IAEA: Global Network of Isotopes in Rivers, available at: [http://www-naweb.iaea.org/naweb/ih/IHS\\_resources\\_gnir.html](http://www-naweb.iaea.org/naweb/ih/IHS_resources_gnir.html) (last access: 30 June 2015), 2012.

IAEA/WMO: Global Network of Isotopes in Precipitation: The GNIP Database, available at: <http://www.iaea.org/water> (last access: 30 June 2015), 2010.

Johnsen, S. J., Dansgaard, W., Clausen, H. B., and Langway, C. C.: Oxygen isotope profiles through the Antarctic and Greenland ice sheets, *Nature*, 235, 429–434, 1972.

Johnsen, S. J., Dahl-Jensen, D., Gundestrup, N., Steffensen, J. P., Clausen, H. B., Miller, H., Masson-Delmotte, V., Sveinbjornsdottir, A. E., and White, J.: Oxygen isotope and palaeotemperature records from six Greenland ice-core stations: Camp Century, Dye-3, GRIP, GISP2, Renland and NorthGRIP, *J. Quaternary Sci.*, 16, 299–307, 2001.

Joussau, S., Sadoury, R., and Jouzel, J.: A general circulation model of water isotope cycles in the atmosphere, *Nature*, 311, 24–29, 1984.

Jouzel, J.: Calibrating the isotopic paleothermometer, *Science*, 286, 910–911, 1999.

Jouzel, J.: A brief history of ice core science over the last 50 yr, *Clim. Past*, 9, 2525–2547, doi:10.5194/cp-9-2525-2013, 2013.

Jouzel, J. and Merlivat, L.: Deuterium and oxygen 18 in precipitation: modeling of the isotopic effects during snow formation, *J. Geophys. Res.*, 89, 11749–11757, 1984.

Jouzel, J., Russell, G. L., Suozzo, R. J., Koster, R. D., White, J. W. C., and Broecker, W. S.: Simulations of the HDO and H<sub>2</sub><sup>18</sup>O atmospheric cycles using the NASA GISS general circulation model: the seasonal cycle for present-day conditions, *J. Geophys. Res.*, 92, 14739–14760, 1987.

## Glacial–interglacial changes of H<sub>2</sub><sup>18</sup>O, HDO and deuterium excess

M. Werner et al.

Title Page

Abstract

Introduction

Conclusions

References

Tables

Figures

◀

▶

◀

▶

Back

Close

Full Screen / Esc

Printer-friendly Version

Interactive Discussion



Jouzel, J., Hoffmann, G., Koster, R. D., and Masson, V.: Water isotopes in precipitation: data/model comparison for present-day and past climates, *Quaternary Sci. Rev.*, 19, 363–379, 2000.

Jouzel, J., Masson-Delmotte, V., Cattani, O., Dreyfus, G., Falourd, S., Hoffmann, G., Minster, B., Nouet, J., Barnola, J. M., Chappellaz, J., Fischer, H., Gallet, J. C., Johnsen, S., Leuenberger, M., Loulergue, L., Luethi, D., Oerter, H., Parrenin, F., Raisbeck, G., Raynaud, D., Schilt, A., Schwander, J., Selmo, E., Souchez, R., Spahni, R., Stauffer, B., Steffensen, J. P., Stenni, B., Stocker, T. F., Tison, J. L., Werner, M., and Wolff, E. W.: Orbital and millennial Antarctic climate variability over the past 800,000 years, *Science*, 317, 793–796, doi:10.1126/science.1141038, 2007.

Jungclaus, J. H., Keenlyside, N., Botzet, M., Haak, H., Luo, J. J., Latif, M., Marotzke, J., Mikolajewicz, U., and Roeckner, E.: Ocean circulation and tropical variability in the coupled model ECHAM5/MPI-OM, *J. Climate*, 19, 3952–3972, 2006.

Kim, S. T. and O'Neil, J. R.: Equilibrium and nonequilibrium oxygen isotope effects in synthetic carbonates, *Geochim. Cosmochim. Ac.*, 61, 3461–3475, 1997.

Knorr, G., Butzin, M., Micochels, A., and Lohmann, G.: A warm Miocene climate at low atmospheric CO<sub>2</sub> levels, *Geophys. Res. Lett.*, 38, L20701, doi:10.1029/2011GL048873, 2011.

Kucera, M., Rosell-Mele, A., Schneider, R., Waelbroeck, C., and Weinelt, M.: Multiproxy approach for the reconstruction of the glacial ocean surface (MARGO), *Quaternary Sci. Rev.*, 24, 813–819, doi:10.1016/j.quascirev.2004.07.017, 2005.

Kurita, N., Noone, D., Risi, C., Schmidt, G. A., Yamada, H., and Yoneyama, K.: Intraseasonal isotopic variation associated with the Madden-Julian Oscillation, *J. Geophys. Res.-Atmos.*, 116, D24101, doi:10.1029/2010JD015209, 2011.

Lee, J.-E., Fung, I., DePaolo, D. J., and Henning, C. C.: Analysis of the global distribution of water isotopes using the NCAR atmospheric general circulation model, *J. Geophys. Res.-Atmos.*, 112, D16306, doi:10.1029/2006JD007657, 2007.

Lee, J.-E., Fung, I., DePaolo, D. J., and Otto-Bliesner, B.: Water isotopes during the Last Glacial Maximum: new general circulation model calculations, *J. Geophys. Res.*, 113, D19109, doi:10.1029/2008JD009859, 2008.

Lee, J.-E., Pierrehumbert, R., Swann, A., and Lintner, B. R.: Sensitivity of stable water isotopic values to convective parameterization schemes, *Geophys. Res. Lett.*, 36, L23801, doi:10.1029/2009gl040880, 2009.

## Glacial–interglacial changes of H<sub>2</sub><sup>18</sup>O, HDO and deuterium excess

M. Werner et al.

Title Page

Abstract

Introduction

Conclusions

References

Tables

Figures

⏪

⏩

◀

▶

Back

Close

Full Screen / Esc

Printer-friendly Version

Interactive Discussion



- LeGrande, A. N. and Schmidt, G. A.: Sources of Holocene variability of oxygen isotopes in paleoclimate archives, *Clim. Past*, 5, 441–455, doi:10.5194/cp-5-441-2009, 2009.
- Lehmann, M. and Siegenthaler, U.: Equilibrium oxygen- and hydrogen-isotope fractionation between ice and water, *J. Glaciol.*, 37, 23–26, 1991.
- 5 Lewis, S. C., LeGrande, A. N., Kelley, M., and Schmidt, G. A.: Water vapour source impacts on oxygen isotope variability in tropical precipitation during Heinrich events, *Clim. Past*, 6, 325–343, doi:10.5194/cp-6-325-2010, 2010.
- Lewis, S. C., LeGrande, A. N., Kelley, M., and Schmidt, G. A.: Modeling insights into deuterium excess as an indicator of water vapor source conditions, *J. Geophys. Res.-Atmos.*, 118, 243–262, doi:10.1029/2012JD017804, 2013.
- 10 Lohmann, G.: Atmospheric and oceanic freshwater transport during weak Atlantic overturning circulation, *Tellus A*, 55, 438–449, 2003.
- Lorius, C., Merlivat, L., Jouzel, J., and Pourchet, M.: 30,000 year isotope climatic record from Antarctic ice, *Nature*, 280, 644–648, 1979.
- 15 Macdonald, R. W., Paton, D. W., Carmack, E. C., and Omstedt, A.: The fresh-water budget and under-ice spreading of Mackenzie River water in the Canadian Beaufort Sea based on salinity and O<sup>18</sup>/O<sup>16</sup> measurements in water and ice, *J. Geophys. Res.*, 100, 895–919, doi:10.1029/94JC02700, 1995.
- Majoube, M.: Fractionnement en oxygène 18 et en deutérium entre l'eau et sa vapeur, *J. Chim. Phys.*, 68, 1423–1436, 1971.
- 20 MARGO Project Members: Constraints on the magnitude and patterns of ocean cooling at the Last Glacial Maximum, *Nat. Geosci.*, 2, 127–132, doi:10.1038/Ngeo411, 2009.
- Marsland, S. J., Haak, H., Jungclaus, J. H., Latif, M., and Roske, F.: The Max-Planck-Institute global ocean/sea ice model with orthogonal curvilinear coordinates, *Ocean Model.*, 5, 91–127, 2003.
- 25 Masson-Delmotte, V., Jouzel, J., Landais, A., Stiévenard, M., Johnsen, S. J., White, J. W. C., Werner, M., Sveinbjornsdottir, A., and Fuhrer, K.: GRIP deuterium excess reveals rapid and orbital-scale changes in Greenland moisture origin, *Science*, 309, 118–121, 2005.
- Masson-Delmotte, V., Kageyama, M., Braconnot, P., Charbit, S., Krinner, G., Ritz, C., Guillard, E., Jouzel, J., Abe-Ouchi, A., Crucifix, M., Gladstone, R. M., Hewitt, C. D., Kitoh, A., LeGrande, A. N., Marti, O., Merkel, U., Motoi, T., Ohgaito, R., Otto-Bliesner, B., Peltier, W. R., Ross, I., Valdes, P. J., Vettoretti, G., Weber, S. L., Wolk, F., and Yu, Y.: Past and future polar

## Glacial–interglacial changes of H<sub>2</sub><sup>18</sup>O, HDO and deuterium excess

M. Werner et al.

Title Page

Abstract

Introduction

Conclusions

References

Tables

Figures

◀

▶

◀

▶

Back

Close

Full Screen / Esc

Printer-friendly Version

Interactive Discussion

amplification of climate change: climate model intercomparisons and ice-core constraints, *Clim. Dynam.*, 26, 513–529, doi:10.1007/S00382-005-0081-9, 2006.

Merlivat, L. and Jouzel, J.: Global climatic interpretation of the deuterium-oxygen 18 relationship for precipitation, *J. Geophys. Res.*, 84, 5029–5033, 1979.

5 Meyer, H., Opel, T., Laepple, T., Dereviagin, A. Y., Hoffmann, K., and Werner, M.: Long-term winter warming trend in the Siberian Arctic during the mid- to late Holocene, *Nat. Geosci.*, 8, 122–125, doi:10.1038/ngeo2349, 2015.

NEEM community members: Eemian interglacial reconstructed from a Greenland folded ice core, *Nature*, 493, 489–494, doi:10.1038/nature11789, 2013.

10 North Greenland Ice Core Project members: High-resolution record of Northern Hemisphere climate extending into the last interglacial period, *Nature*, 431, 147–151, doi:10.1038/Nature02805, 2004.

Paul, A., Mulitza, S., and Pätzold, J.: Simulation of oxygen isotopes in a global ocean model, in: *Use of Proxies in Paleoclimatology: Examples from the South Atlantic*, edited by: Fisher, G. and Wefer, G., Springer, Berlin, Heidelberg, 655–686, 1999.

15 Pfahl, S. and Sodemann, H.: What controls deuterium excess in global precipitation?, *Clim. Past*, 10, 771–781, doi:10.5194/cp-10-771-2014, 2014.

Raddatz, T. J., Reick, C. H., Knorr, W., Kattge, J., Roeckner, E., Schnur, R., Schnitzler, K. G., Wetzel, P., and Jungclaus, J.: Will the tropical land biosphere dominate the climate-carbon cycle feedback during the twenty-first century?, *Clim. Dynam.*, 29, 565–574, doi:10.1007/S00382-007-0247-8, 2007.

20 Risi, C., Bony, S., Vimeux, F., Frankenberg, C., Noone, D., and Worden, J.: Understanding the Sahelian water budget through the isotopic composition of water vapor and precipitation, *J. Geophys. Res.*, 115, D24110, doi:10.1029/2010JD014690, 2010a.

25 Risi, C., Bony, S., Vimeux, F., and Jouzel, J.: Water-stable isotopes in the LMDZ4 general circulation model: model evaluation for present-day and past climates and applications to climatic interpretations of tropical isotopic records, *J. Geophys. Res.-Atmos.*, 115, D12118, doi:10.1029/2009JD013255, 2010b.

30 Roche, D. M. and Caley, T.:  $\delta^{18}\text{O}$  water isotope in the iLOVECLIM model (version 1.0) – Part 2: Evaluation of model results against observed  $\delta^{18}\text{O}$  in water samples, *Geosci. Model Dev.*, 6, 1493–1504, doi:10.5194/gmd-6-1493-2013, 2013.

**Glacial–interglacial changes of H<sub>2</sub><sup>18</sup>O, HDO and deuterium excess**

M. Werner et al.

Title Page

Abstract

Introduction

Conclusions

References

Tables

Figures



Back

Close

Full Screen / Esc

Printer-friendly Version

Interactive Discussion



- Roche, D., Paillard, D., Ganopolski, A., and Hoffmann, G.: Oceanic oxygen-18 at the present day and LGM: equilibrium simulations with a coupled climate model of intermediate complexity, *Earth Planet. Sc. Lett.*, 218, 317–330, doi:10.1016/S0012-821x(03)00700-3, 2004.
- Roche, D. M., Paillard, D., Caley, T., and Waelbroeck, C.: LGM hosing approach to Heinrich Event 1: results and perspectives from data–model integration using water isotopes, *Quaternary Sci. Rev.*, 106, 247–261, doi:10.1016/j.quascirev.2014.07.020, 2014.
- Roeckner, E., Baeuml, G., Bonaventura, L., Brokopf, R., Esch, M., Giorgetta, M., Hagemann, S., Kirchner, I., Kornblueh, L., Manzini, E., Rhodin, A., Schlese, U., Schulzweida, U., and Tompkins, A.: The General Circulation Model ECHAM5, Part I: Model Description, Max Planck Institute for Meteorology, Hamburg, 2003.
- Roeckner, E., Brokopf, R., Esch, M., Giorgetta, M., Hagemann, S., Kornblueh, L., Manzini, E., Schlese, U., and Schulzweida, U.: Sensitivity of simulated climate to horizontal and vertical resolution in the ECHAM5 atmosphere model, *J. Climate*, 19, 3771–3791, 2006.
- Rozanski, K., Araguasaraguas, L., and Gonfiantini, R.: Relation between long-term trends of O<sup>18</sup> isotope composition of precipitation and climate, *Science*, 258, 981–985, 1992.
- Schäfer-Neth, C. and Paul, A.: Gridded Global LGM SST and Salinity Reconstruction, IGBP PAGES/World Data Center for Paleoclimatology, Boulder Data Contribution Series #2003-046, NOAA/NGDC Paleoclimatology Program, Boulder CO, USA, 2003a.
- Schäfer-Neth, C. and Paul, A.: The Atlantic Ocean at the Last Glacial Maximum: 1. objective mapping of the GLAMAP sea-surface conditions, in: *The South Atlantic in the Late Quaternary – Material Budget and Current Systems*, edited by: Wefer, G., Mulitza, S., and Ratmeyer, V., Springer, Berlin, Heidelberg, 531–548, 2003b.
- Schmidt, G. A.: Oxygen-18 variations in a global ocean model, *Geophys. Res. Lett.*, 25, 1201–1204, 1998.
- Schmidt, G. A.: Forward modeling of carbonate proxy data from planktonic foraminifera using oxygen isotope tracers in a global ocean model, *Paleoceanography*, 14, 482–497, 1999.
- Schmidt, G. A., Bigg, G. R., and Rohling, E. J.: Global seawater oxygen-18 database, available at: <http://www.giss.nasa.gov/data/o18data> (last access: 30 June 2015), 1999.
- Schmidt, G. A., LeGrande, A. N., and Hoffmann, G.: Water isotope expressions of intrinsic and forced variability in a coupled ocean-atmosphere model, *J. Geophys. Res.*, 112, D10103, doi:10.1029/2006jd007781, 2007.
- Shackleton, N. J.: Attainment of isotopic equilibrium between ocean water and the benthonic foraminifera genus *Uvigerina*: isotopic changes in the ocean during the last glacial, *Les méth-*



## Glacial–interglacial changes of $H_2^{18}O$ , HDO and deuterium excess

M. Werner et al.

Title Page

Abstract

Introduction

Conclusions

References

Tables

Figures



Back

Close

Full Screen / Esc

Printer-friendly Version

Interactive Discussion



odes quantitatives d'étude des variations du climat au cours du Pleistocène, Gif-sur-Yvette, Colloque international du CNRS, 219, 203–210, 1974.

Shah, A. M., Morrill, C., Gille, E. P., Gross, W. S., Anderson, D. M., Bauer, B. A., Buckner, R., and Hartman, M.: Global speleothem oxygen isotope measurements since the Last Glacial Maximum, *Dataset Papers in Geosciences*, 2013, 548048, doi:10.7167/2013/548048, 2013.

Steen-Larsen, H. C., Johnsen, S. J., Masson-Delmotte, V., Stenni, B., Risi, C., Sodemann, H., Balslev-Clausen, D., Blunier, T., Dahl-Jensen, D., Ellehøj, M. D., Falourd, S., Grindsted, A., Gkinis, V., Jouzel, J., Popp, T., Sheldon, S., Simonsen, S. B., Sjolte, J., Steffensen, J. P., Sperlich, P., Sveinbjörnsdóttir, A. E., Vinther, B. M., and White, J. W. C.: Continuous monitoring of summer surface water vapor isotopic composition above the Greenland Ice Sheet, *Atmos. Chem. Phys.*, 13, 4815–4828, doi:10.5194/acp-13-4815-2013, 2013.

Steen-Larsen, H. C., Masson-Delmotte, V., Hirabayashi, M., Winkler, R., Satow, K., Prié, F., Bayou, N., Brun, E., Cuffey, K. M., Dahl-Jensen, D., Dumont, M., Guillevic, M., Kipfstuhl, S., Landais, A., Popp, T., Risi, C., Steffen, K., Stenni, B., and Sveinbjörnsdóttir, A. E.: What controls the isotopic composition of Greenland surface snow?, *Clim. Past*, 10, 377–392, doi:10.5194/cp-10-377-2014, 2014a.

Steen-Larsen, H. C., Sveinbjörnsdóttir, A. E., Peters, A. J., Masson-Delmotte, V., Guishard, M. P., Hsiao, G., Jouzel, J., Noone, D., Warren, J. K., and White, J. W. C.: Climatic controls on water vapor deuterium excess in the marine boundary layer of the North Atlantic based on 500 days of in situ, continuous measurements, *Atmos. Chem. Phys.*, 14, 7741–7756, doi:10.5194/acp-14-7741-2014, 2014b.

Steen-Larsen, H. C., Sveinbjörnsdóttir, A. E., Jonsson, T., Ritter, F., Bonne, J. L., Masson-Delmotte, V., Sodemann, H., Blunier, T., Dahl-Jensen, D., and Vinther, B. M.: Moisture sources and synoptic to seasonal variability of North Atlantic water vapor isotopic composition, *J. Geophys. Res.-Atmos.*, 120, 5757–5774, doi:10.1002/2015JD023234, 2015.

Stenni, B., Masson-Delmotte, V., Johnsen, S., Jouzel, J., Longinelli, A., Monnin, E., Rothlisberger, R., and Selmo, E.: An oceanic cold reversal during the last deglaciation, *Science*, 293, 2074–2077, 2001.

Stenni, B., Masson-Delmotte, V., Selmo, E., Oerter, H., Meyer, H., Roethlisberger, R., Jouzel, J., Cattani, O., Falourd, S., Fischer, H., Hoffmann, G., Iacumin, P., Johnsen, S. J., Minster, B., and Udisti, R.: The deuterium excess records of EPICA Dome C and Dronning Maud Land ice cores (East Antarctica), *Quaternary Sci. Rev.*, 29, 146–159, doi:10.1016/J.Quascirev.2009.10.009, 2010.



## Glacial–interglacial changes of H<sub>2</sub><sup>18</sup>O, HDO and deuterium excess

M. Werner et al.

Title Page

Abstract

Introduction

Conclusions

References

Tables

Figures

◀

▶

◀

▶

Back

Close

Full Screen / Esc

Printer-friendly Version

Interactive Discussion



- WAIS Divide Project Members: Onset of deglacial warming in West Antarctica driven by local orbital forcing, *Nature*, 520, 661–665, doi:10.1038/nature12376, 2013.
- Wang, Y. J., Cheng, H., Edwards, R. L., An, Z. S., Wu, J. Y., Shen, C. C., and Dorale, J. A.: A high-resolution absolute-dated Late Pleistocene Monsoon record from Hulu Cave, China, *Science*, 294, 2345–2348, doi:10.1126/science.1064618, 2001.
- Wang, Y., Cheng, H., Edwards, R. L., Kong, X., Shao, X., Chen, S., Wu, J., Jiang, X., Wang, X., and An, Z.: Millennial- and orbital-scale changes in the East Asian monsoon over the past 224,000 years, *Nature*, 451, 1090–1093, doi:10.1038/Nature06692, 2008.
- Wei, W. and Lohmann, G.: Simulated Atlantic multidecadal oscillation during the Holocene, *J. Climate*, 25, 6989–7002, doi:10.1175/JCLI-D-11-00667.1, 2012.
- Wei, W., Lohmann, G., and Dima, M.: Distinct modes of internal variability in the global meridional overturning circulation associated with the Southern Hemisphere westerly winds, *J. Phys. Oceanogr.*, 42, 785–801, doi:10.1175/JPO-D-11-038.1, 2012.
- Werner, M. and Heimann, M.: Modeling interannual variability of water isotopes in Greenland and Antarctica, *J. Geophys. Res.*, 107, 4001, doi:10.1029/2001JD900253, 2002.
- Werner, M., Mikolajewicz, U., Heimann, M., and Hoffmann, G.: Borehole vs. isotope temperatures on Greenland: seasonality does matter, *Geophys. Res. Lett.*, 27, 723–726, 2000.
- Werner, M., Heimann, M., and Hoffmann, G.: Isotopic composition and origin of polar precipitation in present and glacial climate simulations, *Tellus Ser. B-Chem. Phys. Meteorol.*, 53, 53–71, 2001.
- Werner, M., Langebroek, P. M., and Carlsen, T.: Stable water isotopes in the ECHAM5 general circulation model: toward high-resolution isotope modeling on a global scale, *J. Geophys. Res.-Atmos.*, 116, D15109, doi:10.1029/2011jd015681, 2011.
- Xu, X.: Variations of oceanic and foraminiferal oxygen isotopes at the present day and the Last Glacial Maximum: equilibrium simulations with an oceanic general circulation model, Universität Bremen, Alfred-Wegener-Institut, available at: <http://epic.awi.de/32264> (last access: 30 June 2015), 2012.
- Xu, X., Werner, M., Butzin, M., and Lohmann, G.: Water isotope variations in the global ocean model MPI-OM, *Geosci. Model Dev.*, 5, 809–818, doi:10.5194/gmd-5-809-2012, 2012.
- Yao, T., Thompson, L., Yang, W., Yu, W., Gao, Y., Guo, X., Yang, X., Duan, K., Zhao, H., Xu, B., Pu, J., Lu, A., Xiang, Y., Kattiel, D. B., and Joswiak, D.: Different glacier status with atmospheric circulations in Tibetan Plateau and surroundings, *Nat. Clim. Change*, 2, 663–667, doi:10.1038/nclimate1580, 2012.

**Glacial–interglacial changes of H<sub>2</sub><sup>18</sup>O, HDO and deuterium excess**

M. Werner et al.

[Title Page](#)[Abstract](#)[Introduction](#)[Conclusions](#)[References](#)[Tables](#)[Figures](#)[⏪](#)[⏩](#)[◀](#)[▶](#)[Back](#)[Close](#)[Full Screen / Esc](#)[Printer-friendly Version](#)[Interactive Discussion](#)

Zaucker, F. and Broecker, W. S.: The influence of atmospheric moisture transport on the fresh water balance of the Atlantic drainage basin: general circulation model simulations and observations, *J. Geophys. Res.*, 97, 2765–2773, doi:10.1029/91JD01699, 1992.

Zhang, X., Lohmann, G., Knorr, G., and Xu, X.: Different ocean states and transient characteristics in Last Glacial Maximum simulations and implications for deglaciation, *Clim. Past*, 9, 2319–2333, doi:10.5194/cp-9-2319-2013, 2013.

Zhang, X., Lohmann, G., Knorr, G., and Purcell, C.: Abrupt glacial climate shifts controlled by ice sheet changes, *Nature*, 512, 290–294, doi:10.1038/nature13592, 2014.

Zhuang, K. and Giardino, J. R.: Ocean cooling pattern at the Last Glacial Maximum, *Adv. Meteorol.*, 2012, 213743, doi:10.1155/2012/213743, 2012.



## Glacial–interglacial changes of H<sub>2</sub><sup>18</sup>O, HDO and deuterium excess

M. Werner et al.

Title Page

Abstract

Introduction

Conclusions

References

Tables

Figures

◀

▶

◀

▶

Back

Close

Full Screen / Esc

Printer-friendly Version

Interactive Discussion



**Table 2.** Selected speleothem sites, reported PI and LGM values of  $\delta^{18}\text{O}_c$  in calcite, and the calculated LGM-PI  $\Delta\delta^{18}\text{O}_{c,\text{LGM-PI}}$  change. All values have been taken from a compilation by Shah et al. (2013) and represent 1000 years-averaged  $\delta^{18}\text{O}_c$  values for both the LGM (defined here as period 19 000 to 22 000 years B.P.) and the most recent 1000 years B.P. (used as an estimate for  $\delta^{18}\text{O}_{c,\text{PI}}$ ). For Botuverá Cave, Gunung Buda National Park, and Sanbao Cave mean values of several reported speleothem records have been calculated. All  $\delta^{18}\text{O}_c$  values refer to the PDB standard.

Cave Name	Lon	Lat	$\delta^{18}\text{O}_{c,\text{PI}}$ [‰]	$\Delta\delta^{18}\text{O}_{c,\text{LGM-PI}}$ [‰]
Botuverá	−49.16	−27.22	−3.2	−0.3
Cold Air	29.11	−24.02	−4.3	1.2
Gunung Buda	114.80	4.03	−9.3	1.7
Jerusalem West	35.15	31.78	−4.9	1.4
NWSI	172.00	−42.00	−3.2	0.3
Sanbao	110.43	31.67	−8.8	0.1
Sofular	31.93	41.42	−8.1	−4.5
Soreq	35.03	31.45	−5.4	2.2

## Glacial–interglacial changes of $\text{H}_2^{18}\text{O}$ , HDO and deuterium excess

M. Werner et al.

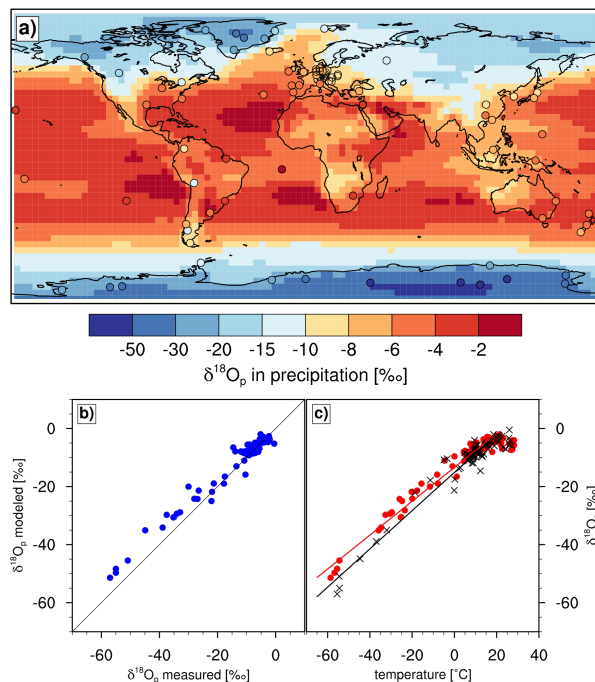


**Figure 1.** (a) Global distribution of simulated and observed annual mean  $\delta^{18}\text{O}_p$  values in precipitation. The background pattern shows the  $\delta^{18}\text{O}_p$  distribution as simulated by the ECHAM5/MPI-OM model setup. Data from 70 GNIP stations (see text), from 8 speleothem records (Table 1) and 16 ice core records (Table 2) are plotted as coloured symbols. (b) Modelled vs. observed annual mean  $\delta^{18}\text{O}_p$  at the different GNIP, speleothem, and ice cores sites. The black line represents the 1 : 1 line indicating a perfect model fit. (c) Observed (black crosses) and modelled (filled red circles) spatial  $\delta^{18}\text{O}_p$ – $T$  relationship for annual mean values of  $T$  and  $\delta^{18}\text{O}_p$  at 71 sites, where observed annual mean temperatures are below  $+20^\circ\text{C}$ . The black (red) solid line represents a linear fit of the observed (modelled) data set.

Title Page

Abstract

Introduction

Conclusions

References

Tables

Figures

◀

▶

◀

▶

Back

Close

Full Screen / Esc

Printer-friendly Version

Interactive Discussion



## Glacial–interglacial changes of $\text{H}_2^{18}\text{O}$ , HDO and deuterium excess

M. Werner et al.

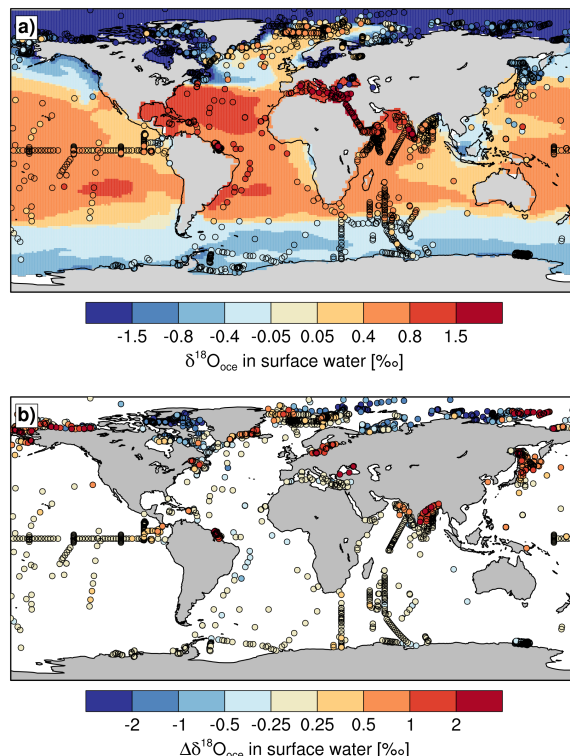


**Figure 2.** (a) Global distribution of simulated and observed annual mean  $\delta^{18}\text{O}_{\text{Oce}}$  values in ocean surface waters (mean over depth interval between surface and 10 m). The background pattern shows the  $\delta^{18}\text{O}_{\text{Oce}}$  distribution as simulated by the ECHAM5/MPI-OM model setup. Data entries from the GISS database are plotted as coloured symbols. (b) Anomaly plot for the difference of the mean modelled vs. observational values ( $\Delta\delta^{18}\text{O}_{\text{Oce}} = \delta^{18}\text{O}_{\text{Oce}} - \delta^{18}\text{O}_{\text{GISS}}$ ) at the positions of the GISS data entries. For the calculation of  $\Delta\delta^{18}\text{O}_{\text{Oce}}$ , the month of sampling has been considered (see text for details).

Title Page

Abstract

Introduction

Conclusions

References

Tables

Figures

◀

▶

◀

▶

Back

Close

Full Screen / Esc

Printer-friendly Version

Interactive Discussion





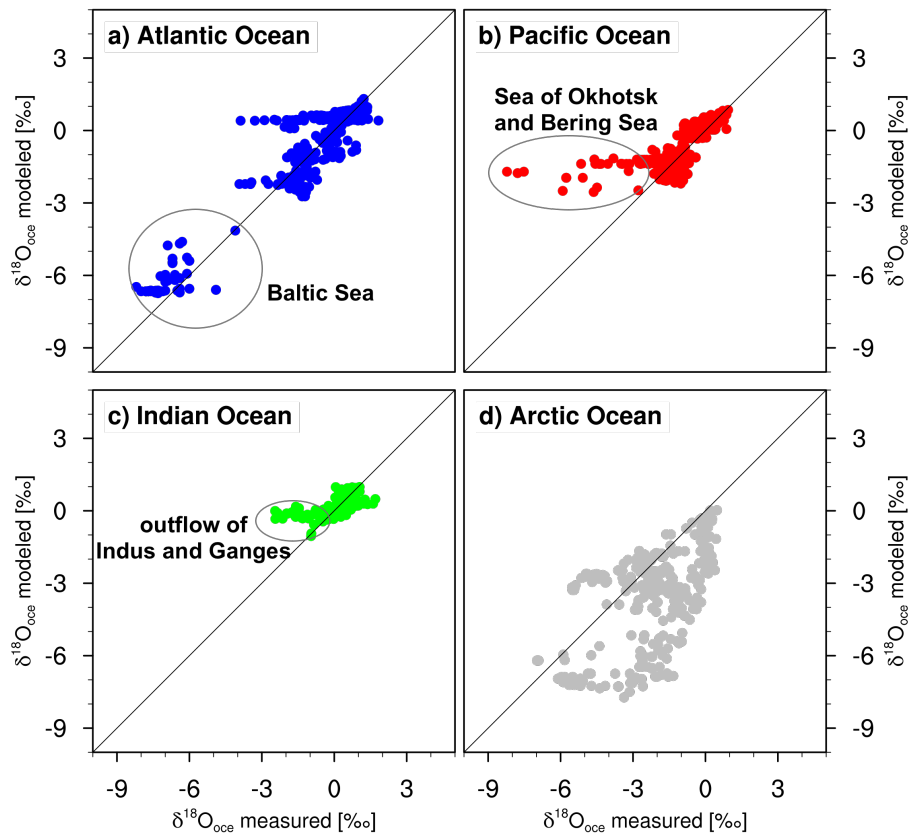


**Figure 3.** Scatter plots of observed present-day  $\delta^{18}\text{O}_{\text{oce}}$  values from the GISS database vs. modelled  $\delta^{18}\text{O}_{\text{oce}}$  values of the PI simulation for following basins: **(a)** Atlantic Ocean, **(b)** Pacific Ocean, **(c)** Indian Ocean, **(d)** Arctic Ocean. The black lines represent the 1 : 1 line indicating a perfect model fit.

## Glacial–interglacial changes of $\text{H}_2^{18}\text{O}$ , HDO and deuterium excess

M. Werner et al.

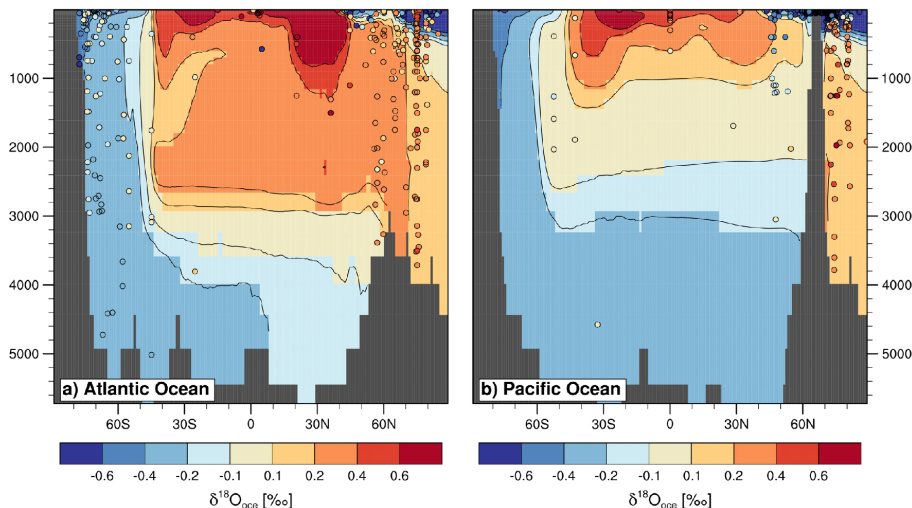


**Figure 4.** Background pattern: Meridional section of the simulated  $\delta^{18}\text{O}_{\text{oce}}$  values in **(a)** the Atlantic (zonal mean over  $60^\circ\text{W}$  to  $0^\circ\text{W}$ ), **(b)** the Pacific (zonal mean over  $150^\circ\text{E}$  to  $110^\circ\text{W}$ ). Data entries from the GISS database are plotted as coloured symbols. For improved readability, only an arbitrary subset of 300 data entries from the complete available GISS data set (Atlantic Ocean:  $n = 5811$ , Pacific Ocean:  $n = 2985$ ) is shown in each panel.

Title Page

Abstract

Introduction

Conclusions

References

Tables

Figures

◀

▶

◀

▶

Back

Close

Full Screen / Esc

Printer-friendly Version

Interactive Discussion



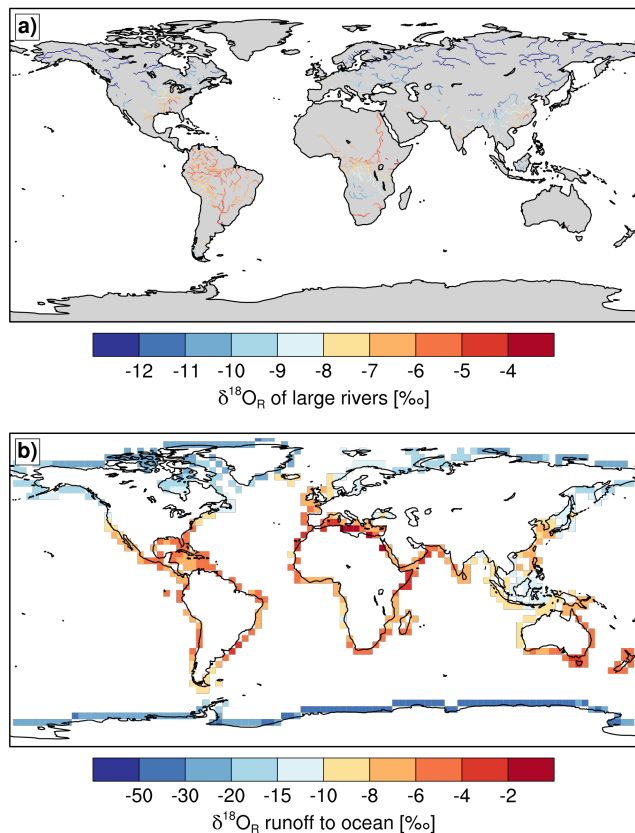


**Figure 5.** Global distribution of the simulated annual mean  $\delta^{18}\text{O}_R$  signal in **(a)** large rivers, **(b)** surface water runoff from coastal grid points into the oceans, as simulated by the hydrological discharge model (HD model) within the ECHAM5/MPI-OM setup.

Glacial–interglacial changes of  $\text{H}_2^{18}\text{O}$ , HDO and deuterium excess

M. Werner et al.

Title Page

Abstract

Introduction

Conclusions

References

Tables

Figures

◀

▶

◀

▶

Back

Close

Full Screen / Esc

Printer-friendly Version

Interactive Discussion



## Glacial–interglacial changes of $H_2^{18}O$ , HDO and deuterium excess

M. Werner et al.

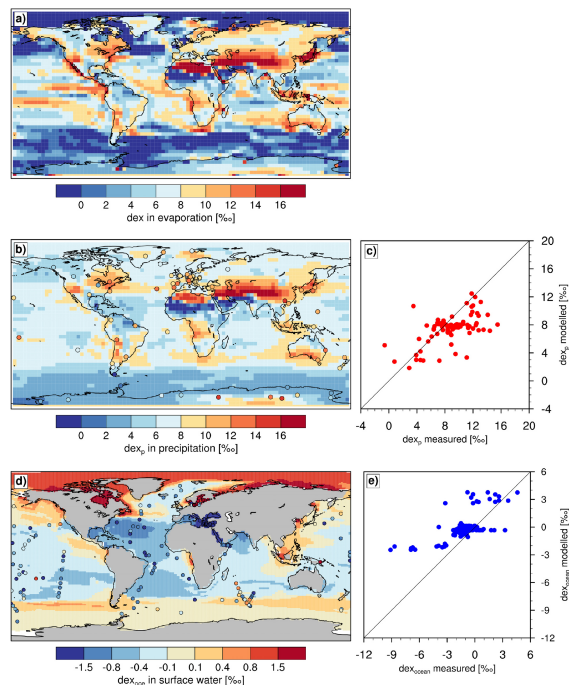


**Figure 6.** Global distribution of simulated and observed annual mean deuterium excess (dex) values in **(a)** evaporation, **(b)** precipitation, **(d)** ocean surface waters. The background pattern shows the dex distribution as simulated by ECHAM5/MPI-OM. In **(b)**, data from 70 GNIP stations, and 21 ice cores from Greenland and Antarctica are plotted as coloured symbols. In **(d)**, 153 data entries from the GISS database are plotted as coloured symbols. Comparison of observed present-day dex values in **(c)** precipitation (red symbols), and **(e)** in ocean surface waters (blue symbols) vs. the corresponding modelled dex values of the PI simulation. The black lines in **(c)** and **(e)** represent the 1 : 1 line indicating a perfect model fit.

Title Page

Abstract

Introduction

Conclusions

References

Tables

Figures

◀

▶

◀

▶

Back

Close

Full Screen / Esc

Printer-friendly Version

Interactive Discussion



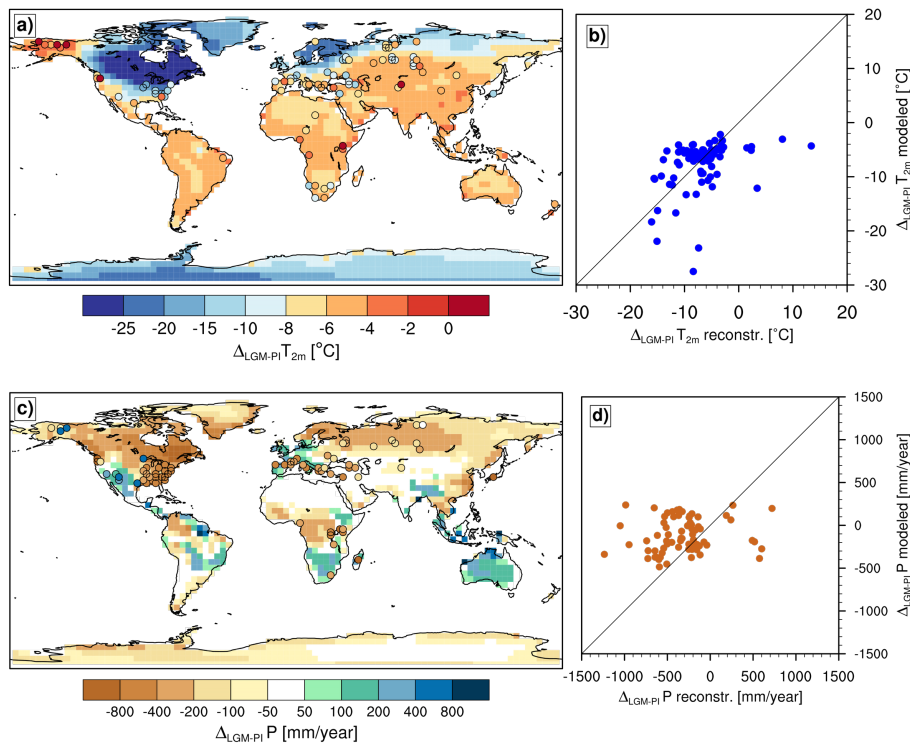


**Figure 7.** (a) Background pattern: simulated global pattern of annual mean surface temperature ( $T_{2m}$ ) changes between the LGM and PI climate. Pollen-based reconstructed temperature changes by Bartlein et al. (2011) are shown as coloured symbols. (b) Comparison of reconstructed temperature changes shown in (a) vs. the simulated LGM-PI cooling at the sample locations. The black line represents the 1 : 1 line indicating a perfect model fit. (c) Simulated global pattern of annual mean precipitation changes between the LGM and PI climate. (d) Comparison of reconstructed precipitation changes shown in (b) vs. the simulated LGM-PI change at the sample locations. The black line represents the 1 : 1 line indicating a perfect model fit.

## Glacial–interglacial changes of $\text{H}_2^{18}\text{O}$ , HDO and deuterium excess

M. Werner et al.

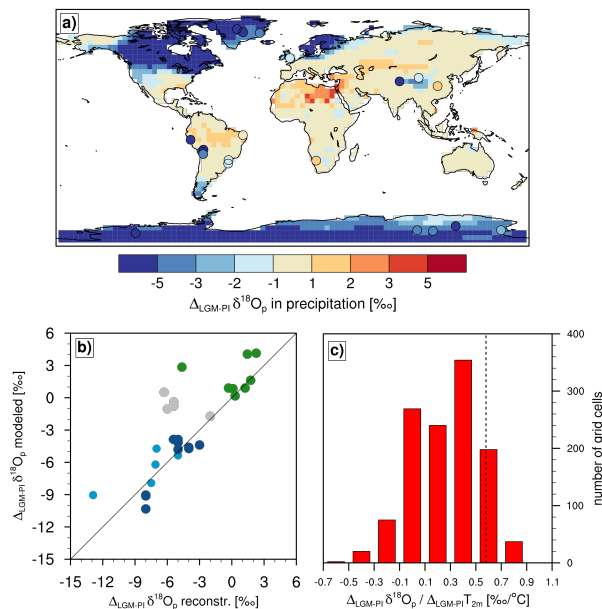


**Figure 8.** (a) Background pattern: simulated global pattern of annual mean  $\delta^{18}\text{O}_p$  changes between the LGM and PI climate. Reconstructed  $\delta^{18}\text{O}_p$  changes of ice cores and  $\delta^{18}\text{O}_c$  in speleothems are shown as coloured symbols. (b) Comparison of reconstructed  $\delta^{18}\text{O}$  changes shown in (a) vs. the simulated LGM-PI  $\delta^{18}\text{O}$  changes at the same locations. Reconstructed  $\delta^{18}\text{O}_p$  anomalies stem from the following archives: Antarctica (dark blue), Greenland (light blue), and tropical ice cores (grey). For speleothems, reconstructed and simulated  $\delta^{18}\text{O}_c$  changes are shown (green). The black line represents the 1 : 1 line indicating a perfect model fit. (c) Histogram of calculated temporal LGM-PI  $\delta^{18}\text{O}_p$ - $T$  gradients for all grid cells with (i) an annual mean PI temperature below  $+20^\circ\text{C}$ , and (ii) a simulated LGM-PI cooling of at least  $-2^\circ$ . The dashed line indicates the modelled PI spatial  $\delta^{18}\text{O}_p$ - $T$  gradient ( $0.58\text{‰}\text{C}^{-1}$ ).

## Glacial–interglacial changes of $\text{H}_2^{18}\text{O}$ , HDO and deuterium excess

M. Werner et al.

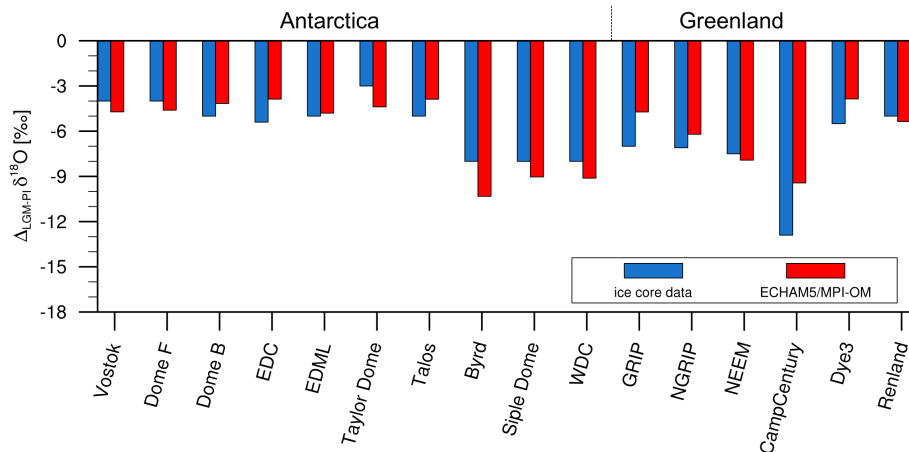


**Figure 9.** Comparison of annual mean LGM  $\delta^{18}\text{O}_p$  anomalies measured in ice cores from Antarctica and Greenland (blue bars) vs. the simulated ECHAM5/MPI-OM LGM-PI  $\delta^{18}\text{O}_p$  changes (red bars) at the ice core locations.

Title Page

Abstract

Introduction

Conclusions

References

Tables

Figures

⏪

⏩

◀

▶

Back

Close

Full Screen / Esc

Printer-friendly Version

Interactive Discussion



## Glacial–interglacial changes of $\text{H}_2^{18}\text{O}$ , HDO and deuterium excess

M. Werner et al.

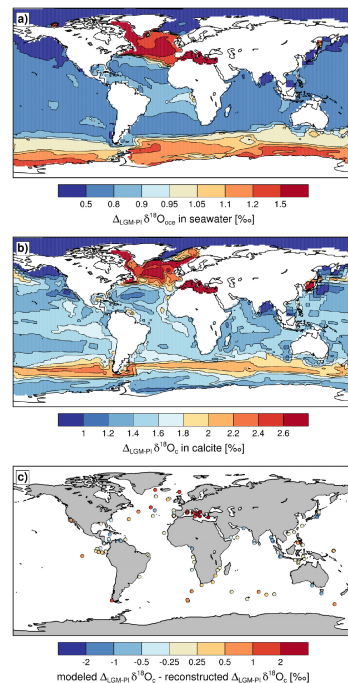


**Figure 10.** (a) Simulated global pattern of annual mean  $\delta^{18}\text{O}_{\text{occe}}$  changes in ocean surface waters (0–50 m depth) between the LGM and PI climate. (b) Calculated global pattern of annual mean  $\delta^{18}\text{O}_c$  changes in calcite in ocean surface waters between the LGM and PI climate. The  $\delta^{18}\text{O}_c$  values are derived from the simulated  $\delta^{18}\text{O}_{\text{occe}}$  changes shown in (a) and the modelled LGM-PI ocean temperature changes (see text for details). (c) Difference between simulated LGM-PI  $\delta^{18}\text{O}_c$  changes and LGM-Late Holocene  $\delta^{18}\text{O}_c$  anomalies of a compilation of 114 planktic foraminifera data entries compiled by Caley et al. (2014).



## Glacial–interglacial changes of $\text{H}_2^{18}\text{O}$ , HDO and deuterium excess

M. Werner et al.

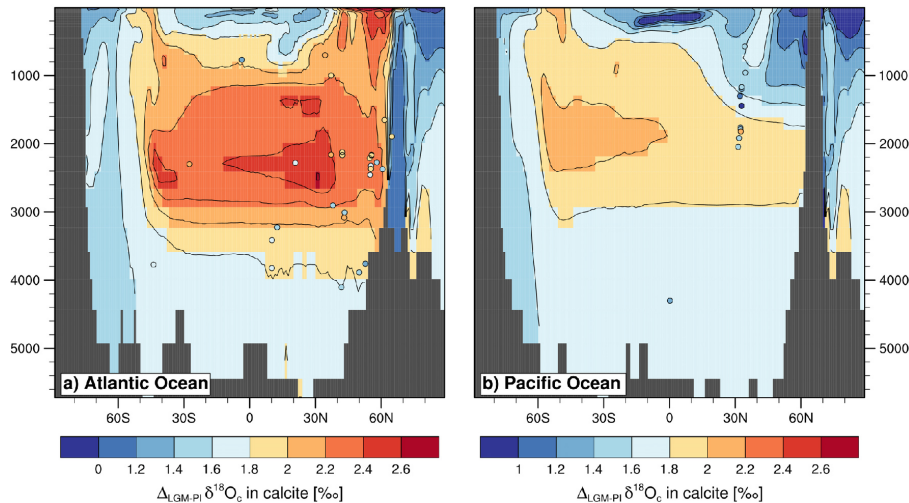


**Figure 11.** Background pattern: meridional section of the simulated annual mean LGM-PI  $\delta^{18}\text{O}_c$  in calcite changes in (a) the Atlantic (zonal over  $60^\circ\text{W}$  to  $0^\circ\text{W}$ ), (b) the Pacific (zonal mean over  $150^\circ\text{E}$  to  $110^\circ\text{W}$ ). Geographically related data entries from a compilation of 115 LGM-Late Holocene  $\delta^{18}\text{O}_c$  anomalies of benthic foraminifera data compiled by Caley et al. (2014) are plotted as coloured symbols (Atlantic Ocean:  $n = 29$ ; Pacific Ocean:  $n = 12$ ) in each panel.

Title Page

Abstract

Introduction

Conclusions

References

Tables

Figures

◀

▶

◀

▶

Back

Close

Full Screen / Esc

Printer-friendly Version

Interactive Discussion



## Glacial–interglacial changes of $H_2^{18}O$ , HDO and deuterium excess

M. Werner et al.

Title Page

Abstract

Introduction

Conclusions

References

Tables

Figures

◀

▶

◀

▶

Back

Close

Full Screen / Esc

Printer-friendly Version

Interactive Discussion

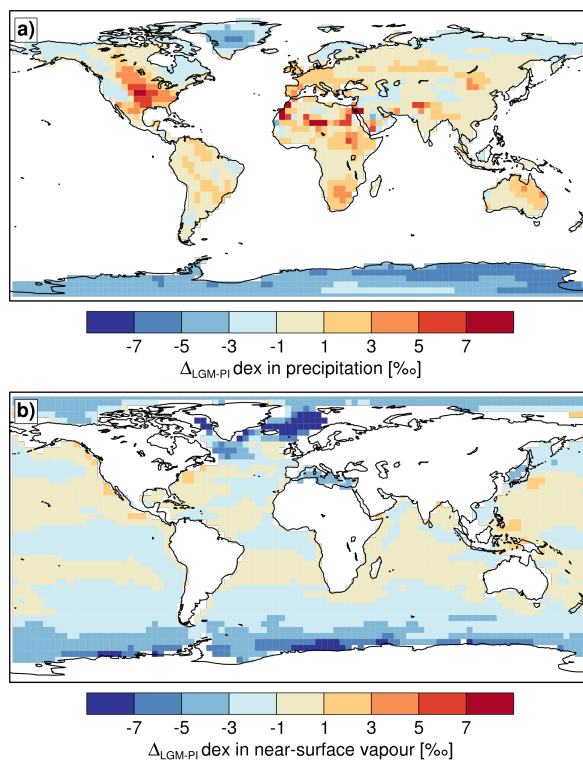


**Figure 12.** Global distribution of simulated annual mean LGM-PI deuterium excess (dex) changes in (a) continental precipitation, (b) water vapour of the lowest atmospheric model layer above the ocean surface.

## Glacial–interglacial changes of $H_2^{18}O$ , HDO and deuterium excess

M. Werner et al.

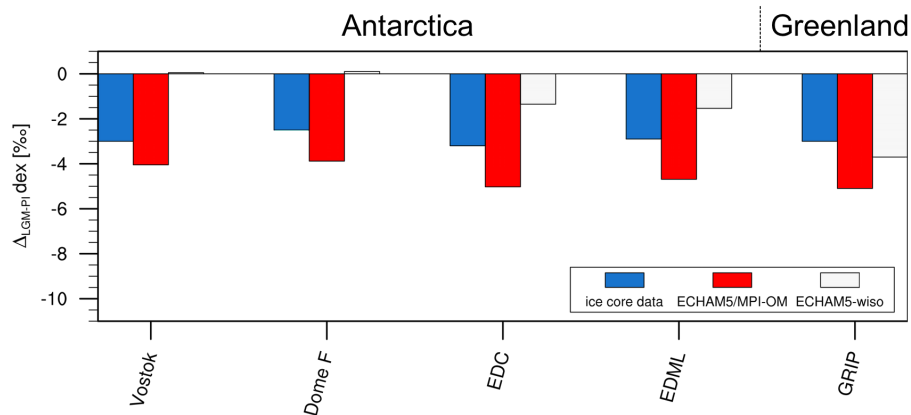


**Figure 13.** Comparison of annual mean LGM dex anomalies measured in ice cores from Antarctica and Greenland (blue bars) vs. simulated LGM-PI dex changes (ECHAM5/MPI-OM: red bars; ECHAM5-wiso: light grey bars) at the ice core locations.

Title Page

Abstract

Introduction

Conclusions

References

Tables

Figures

⏪

⏩

◀

▶

Back

Close

Full Screen / Esc

Printer-friendly Version

Interactive Discussion



